COLLEGE OF ENGINEERING
UNIVERSITY OF WISCONSIN-MADISON

Department of Materials Science & Engineering
Professor John H. Perepezko
1509 University Ave.
Madison, WI 53706-1595
perepezk@engr.wisc.edu
http://www.engr.wisc.edu/mse
Phone: 608/263-1678
Fax: 608/262-8353

January 28, 2021

Defense Technical Information Center
8725 John J Kingman Road
Ste 0944
Fort Belvoir, VA 22060-6218

Gentlemen:

I am enclosing the final technical report with the SF298 form for our project on "Environmental Resistant Coatings for High Temperature Mo Silicides" under award number N00014-17-1-2575. I would be grateful to receive a confirmation of receipt by email at perepezk@engr.wisc.edu

Sincerely,

John H. Perepezko

IBM-Bascom Professor

REPORT DOCUMENTATION PAGE

Form Approved
OMB No. 0704-0188

The public reporting burden for this collection of information is estimated to average 1 hour per response, including the time for reviewing instructions, searching existing data sources, gathering and maintaining the data needed, and completing and reviewing the collection of information. Send comments regarding this burden estimate or any other aspect of this collection of information, including suggestions for reducing the burden, to Department of Defense, Washington Headquarters Services, Directorate for Information Operations and Reports (0704-0188), 1215 Jefferson Davis Highway, Suite 1204, Arlington, VA 22202-4302. Respondents should be aware that notwithstanding any other provision of law, no person shall be subject to any penalty for failing to comply with a collection of information if it does not display a currently valid OMB control number.
PLEASE DO NOT RETURN YOUR FORM TO THE ABOVE ADDRESS.

1. REPORT DATE *(DD-MM-YYYY)*	2. REPORT TYPE	3. DATES COVERED *(From - To)*
01/28/2021	Final Technical	05/01/2017-09/30/2020

4. TITLE AND SUBTITLE
Environmental Resistant Coatings for High Temperature Mo Silicide Alloys

5a. CONTRACT NUMBER

5b. GRANT NUMBER
N00014-17-1-2575

5c. PROGRAM ELEMENT NUMBER

6. AUTHOR(S)
Professor John H. Perepezko

5d. PROJECT NUMBER
1000007123

5e. TASK NUMBER

5f. WORK UNIT NUMBER

7. PERFORMING ORGANIZATION NAME(S) AND ADDRESS(ES)
University of Wisconsin-Madison
Department of Materials Science and Engineering
1509 University Avenue
Madison, WI 53706

8. PERFORMING ORGANIZATION REPORT NUMBER

9. SPONSORING/MONITORING AGENCY NAME(S) AND ADDRESS(ES)
Dr. David A. Shifler
Office of Naval Research
ONR 332
875 North Randolph
Arlington, VA 22203-1995

10. SPONSOR/MONITOR'S ACRONYM(S)
ONR

11. SPONSOR/MONITOR'S REPORT NUMBER(S)

12. DISTRIBUTION/AVAILABILITY STATEMENT
Unlimited

13. SUPPLEMENTARY NOTES

14. ABSTRACT
In-situ reaction processing and kinetic biasing of diffusion paths in the pack cementation synthesis of robust coatings in the Mo-Si-B system has been demonstrated as an effective approach to achieve stable compatibility between coating layer/ substrate alloy combinations. We have focused on a number of critical coating applications, namely (1) The capability of MoSiB coatings to suppress hot corrosion attack, (2) The oxidation resistance of MoSiB coatings in a water vapor environment (3) The use of MoSiB coatings for environmental protection of SiC/C Composites (4) The influence of minor alloying additions such as Al on the oxidation response of MoSiB coatings (5) Raman Spectroscopy evaluation of coatings.

15. SUBJECT TERMS
Oxidation resistant coatings, High temperature Mo-Si-B alloys, Diffusion pathways, Kinetic bias, Pack cementation, SiC/C composites, water vapor, hot corrosion,Raman Spectroscopy.

16. SECURITY CLASSIFICATION OF:			17. LIMITATION OF ABSTRACT	18. NUMBER OF PAGES	19a. NAME OF RESPONSIBLE PERSON
a. REPORT	b. ABSTRACT	c. THIS PAGE			Professor John H Perepezko
					19b. TELEPHONE NUMBER *(Include area code)*
U	U	U	UU	48	608-263-1678

Table of Contents

Technical Approach and Justification

1. Introduction

The challenges of a high temperature environment (T>1400°C) impose severe material performance constraints in terms of melting point, oxidation resistance and structural functionality. A number of ceramic materials, intermetallic compounds and refractory metals with high melting temperature are available as material choices. However, in a single component, single-phase form, these materials rarely satisfy all the above requirements because of the brittleness of ceramic materials and intermetallic compounds at low temperatures and the oxidation problems and poor creep resistance of refractory metals at high temperatures. In this respect the evolutionary development of high temperature alloys over the past 4-5 decades represents a remarkable achievement and provides important lessons to guide future materials design efforts. One clear message is the importance of multiphase microstructures and the capability to control phase fractions and morphologies within the overall structure [Ros 87, Sto 87, Dys 90]. The flexibility in microstructure control has been shown to be critical in tailoring alloy performance in order to satisfy a number of mechanical property requirements that sometimes present conflicting demands [Kim 91, Dim 92]. Besides the essential structural requirements, elevated temperatures also often involve aggressive environments that require a material to display an inherent oxidation protection that can be enhanced further by coating [Mai 79].

In terms of metallic system candidates there are several high melting temperature intermetallics, but there is a much smaller number of intermetallic phases that offer a level of inherent environmental resistance. At elevated temperature, alloy phases that contain Al or Si are most attractive for developing stable Al_2O_3 and SiO_2 coatings. Moreover, above about 1300°C, SiO_2 films are preferred since the parabolic rate constant for oxidation is lower for SiO_2 than for Al_2O_3 [Bir 83]. In fact, this selection is supported by the superior oxidation resistance available with monolithic $MoSi_2$ where a SiO_2 surface provides for useful operation up to about 1700°C (i.e. 0.8 T_m). At high temperatures the creep strength of $MoSi_2$ is insufficient and at low temperature it is brittle [Boe 92, Sha 92, Vas 92]. Since most of the single-phase intermetallic silicides experience a relatively low ambient fracture toughness, significant efforts to remedy this deficiency have been geared toward the development of *in-situ* ductile phase-toughened intermetallic composites [Men 93, Str 93, Sha 95]. The requirement of a thermodynamically compatible two-phase mixture in binary systems nevertheless presents a serious problem due to limited availability of suitable components [Sha 95]. In the case of $MoSi_2$, for instance, there are no high melting ductile phases that have been identified to be in equilibrium with $MoSi_2$ which is a serious issue in structural applications due to its brittle nature.

At the same time, the multiphase microstructures that can be developed in the Mo-Si-B system involving the high melting temperature (>2100°C) ternary-based intermetallic Mo_5SiB_2 (T_2) offer an attractive option particularly due to the superior oxidation resistance of the Mo-based silicides [Nun 97, Per 97]. In terms of the available phase combinations in the Mo-Si-B system that are indicated in the phase diagram in Figure 1, the two-phase combination of Mo(ss) +T_2

offers enhanced toughening [Nun 00] due to a precipitation of Mo(ss) that can be produced within the T_2 phase [Sak 98, Sak 99, Sch 99] while three phase alloys comprised of Mo(ss), T_2 and Mo_3Si or Mo_3Si, T_2 and Mo_5Si_3 (see the Mo-Si-B isothermal sections at 1600°C & 1850°C in Figure 1) offer favorable oxidation resistance [Tho 93, Sch 98, Sch 99]. A focal point of the microstructural designs is clearly the T_2 phase that is central to the phase selections that promote high temperature stability and robust microstructures.

A coating system represents a multifunctional and multiphase system with a large internal interface area. The application of mechanics based design concepts has imparted useful engineering properties to systems with components that individually have limited performance. In fact, it has been possible to design useful values of toughness into brittle/ductile systems by programming the interface characteristics. Indeed, it is fair to state that a key part of the mechanics - based design innovations have focused on the internal interfaces. However, even with the advances in design, the link between design, structural stability, processing and performance has not been fully applied. This has been the basis for a new paradigm of in-situ reaction processing. The motivation for this evolution is both economic as well as representing the best elements of design, processing and structural stability control. At the same time, the evolution in processing strategy has lead to the realization that the principles and concepts involved in the development of in-situ reaction processing can be applied to a number of other materials systems, specifically coatings that are an important component of many engineering materials systems [Per 93].

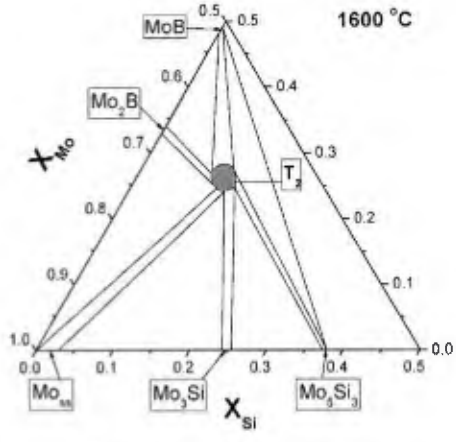

Figure 1. Isothermal section of Mo-Si-B phase diagram at 1600°C [Kim 06].

In principle, the development and application of reaction control concepts in coatings provides an effective guideline for designing compatible interfaces. In terms of oxidation performance, the Mo-Si-B ternary system offers an attractive option since boron additions enhance significantly the oxidation resistance of metal-rich binary silicides [Tho 93] and the Mo phase together with the equilibrium ternary phase (Mo_5SiB_2) have demonstrated the ductile phase toughening mechanism, [Now 57, Nun 97, Per 97]. At the same time, at high temperature the Mo-Si-B system tends to produce favorable borosilica layers which exhibit useful oxidation resistance [Men 93], comparable to other silicides. From the available experience on the oxidation behavior

of Mo-Si-B alloys that has been reported it is evident bo the kinetics are sensitive to composition and the addition of higher order components. Single phase T_2 compositions exhibit a high metal recession rate of over 3000μm/100 hr at 1100°C. However, three phase alloys based upon $Mo+T_2+Mo_3Si$ with Ti or Hf additions exhibit recession rates of less than 100 μm/100 hr at 1100°C. Moreover, [Woo 03] the doping of three phase alloys with small amounts of Fe, Ni or Co was reported to reduce the recession rate to about 1 μm/ hr at 1370°C that is well below the design goal of 10 mil/100hr (i.e. 250μm/100 hr). However, at lower temperatures the doping additions were ineffective in suppressing degradation. Clearly, the understanding of the large sensitivity of the oxidation rate to alloy composition is a critical issue. Moreover, since the alloy compositions that exhibit the lowest oxidation rate will most likely not yield optimum performance for the mechanical properties, it is important to develop oxidation resistant coatings that are robust and compatible. An effective strategy to address this challenge is based upon in-situ reaction processing to develop coating systems that are thermodynamically compatible with the base alloy and also incorporate an inherent capability for repair.

The development of coating layers, such as Thermal Barrier Coatings (TBCs) which includes multifunctional multilayers, indicates further the importance of a fabricating compatible interface designs for the coatings and the substrate materials as well. In fact, beneath a TBC layer, a thermally grown oxide (TGO) that forms upon oxidation exposure has been identified as a primary failure mode in the TBC system, implying that oxidation control together with stable interface design are critical for successful TBC layer design.

One useful design concept that has been developed for multilayer systems is the functional grading (FGM) concept, which is based on a gradual composition variation between the incompatible constituents [Smi 84; Kie 91]. In principle, in-situ reaction processing together with FGM would evolve a promising and a natural built-in compatibility and in addition a self-repair mechanism. At the same time, such designs offer challenges in materials synthesis and processing in terms of optimizing the reaction kinetics, phase structure and product morphology development [Rap 73, Per 93].

In the current studies these challenges are being addressed in several focus areas. For example, the evolution of the interdiffusion reaction that initiates at interfaces involves a particular reaction path, which is related to the diffusion path in the system [Kir 87]. Understanding the kinetics of the diffusion path and its control are essential to modifying the overall microstructural morphology resulting from a modified phase sequence [Per 98]. Moreover, it is apparent that diffusion through the product phase is an essential feature of reactive phase formation. For example, in the current studies on oxidation and coating reactions in Mo-Si-B alloys, it has been established that a strategy based on a kinetic biasing can be a most effective approach in controlling the diffusion pathway and an important component in modifying the microstructural morphology of the various intermediate layers that develop during interface reactions.

2. Background

2.1 Evolution of Phase Stability Hierarchy and Interdiffusion Reactions

As a starting point in the evaluation of phase compatibility in composite systems it is essential to consider the phase stability. This is illustrated in a model ternary system such as that shown in Figure 2. In this system four binary compounds: α, β, δ, and γ exist as well as the primary solid solution phases. While the basic thermodynamic stability is very important, it does not yield the reaction sequence between phases in a multiphase system. For example, as indicated in Figure 2 in an initial pairing of the phase mixture of γ and B there are several possible combinations of reaction products all of which represent stable pairings of the two phase mixtures, but evolve through different phase sequencing pathways. In order to assess which of these reaction pathways is selected, it is important to determine the interdiffusion path and reaction kinetics associated with the reduction in system free energy during reaction. At the same time, the multiplicity of pathways offers a potential strategy for altering the sequence of phases into a desired pathway. Initially, if a product δ phase is desired between γ and B, it is useful to consider biasing the kinetics of the diffusion pathway using an excess flux of A. Then, the δ phase is included in the reaction pathway. It also appears that the strategy would be most effective if it also occurs with a continuous decrease in the chemical potentials of the mobile components [Loo 85] otherwise as discussed by van Loo activity gradients can be present and the design would represent a transient condition. Of course, such a transient behavior may be of an extended duration which can be designed to exceed the service lifetime if the diffusion process controlling modification of the phase layers is sluggish.

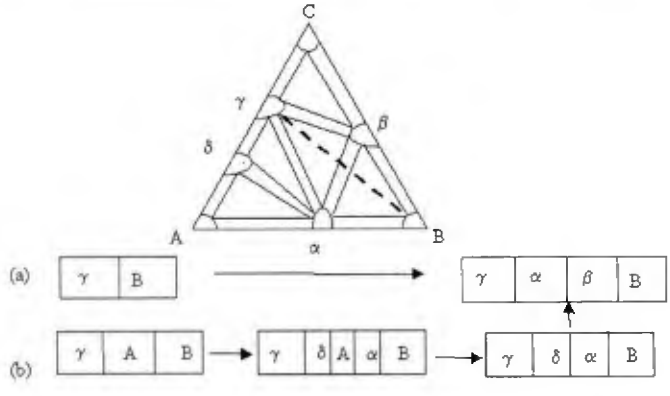

Figure 2. Potential reaction layer formation in a γ / B and γ / A / B diffusion couple involving a stable pairing of phases.

When the reaction kinetics are favorable the initial components can be converted into stable combinations by displacement reactions [Wag 38, Rap 73] such as a displacement for oxides : A+BO→AO+B . The sequence and arrangement of phases has an important influence on the morphology of the resulting products [Wag 38]. For an initial layered arrangement of A and BO a layered arrangement of AO, and B can develop by sequential reaction. Alternatively, an aggregate arrangement (i.e. interwoven or lamellar) of AO and B can develop by coupled growth

when the growth of B is controlling [Rap 73]. With either morphology class, a stable product structure is established by the displacement reaction [Hen 93]. The issue of morphology control can be a deciding factor in optimizing the performance of a coating system once the correct phase structure has been established.

The morphology of the interfaces during in-situ reaction is one of the important issues for coatings materials design [Loo 83, Ram 85]. Depending on the relative fluxes of the different components to the interface, the shape of the interface can be modified between limits ranging from a planar to a fully interwoven configuration. In coatings, an interwoven microstructure can be used in a graded layering to modify the structure in a smooth manner and to minimize the build up of stresses which lead to cracking and spalling of coatings. Moreover, it is important to realize that the diffusion path provides not only critical information on phase sequencing during interdiffusion reactions, but also essential information on the relative fluxes of the separate components which can be used to control interface morphology. With this in mind it is also evident that altering the diffusion path to change the phase sequence will also have an influence on the resultant morphology of the phase combinations; thus, both factors must be considered together and indeed can be used in useful microstructural designs.

While the interface stability concept is applicable to the oxidation of metal /alloy combinations, it is also worthwhile to examine the governing factors for the oxide scale formation. In fact, the oxidation behavior of alloys increases the complexity, since multiple steps are involved. For most oxidation reactions, the superficial scale separates from the reactants so that the final products are not usually produced simultaneously [Whi 83]. In many cases, the diffusion rate of the metal component is one of the key factors for protective oxide layer formation. However, in practice, the competition of metal component vs. oxygen diffusion rate together with the soundness of the oxide scale layer determines the oxide scale formation.

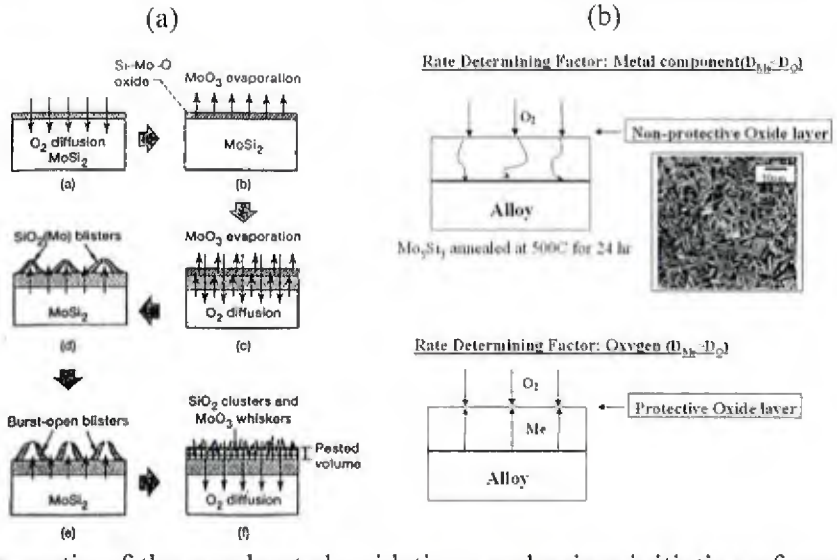

Figure 3. a) Schematic of the accelerated oxidation mechanism initiation of pest degradation on $MoSi_2$ at 500°C [Cho 93]. b) Schematic illustration of critical oxidation behavior (SEM micrograph shows the development of pest process (Mo_5Si_3 alloy annealed at 500°C for 24 hr)).

One example of the kinetic competition that is of special relevance to the behavior of Mo-Si-B alloys is the oxidation behavior of Mo-Si alloys at low temperature (Figure 3a). Upon exposure in air, MoO_3 forms and volatilizes from the reaction of oxygen and Mo, leaving a SiO_2 rich layer. The defects of the surface SiO_2 layer allow oxygen to penetrate through the alloy, eventually the condensed MoO_3 (usually platelet shape) together with SiO_2 remains on the surface. However, at high temperature, the diffusion of Si from the alloy becomes more rapid to the oxide layer and can maintain a SiO_2 layer. This behavior, of course, is associated with the viscosity of the oxide scale. The schematic illustration representing the critical oxygen behavior is shown in Figure 4b including the oxidized microstructure of Mo_5Si_3 following oxidation at 500°C for 24 hr. The microstructure implies severe oxygen attack can degrade an alloy with only limited time exposure. This is commonly called "pesting". In order to address this behavior several approaches may be considered to improve oxidation resistance such as developing coating strategies together with alloy design. An effective solution has been developed in the current program.

2.2 Pathways – Multicomponent Systems

One important useful design tool in the synthesis of a reliable and stable coating system follows from the application of composition gradients during the initial fabrication. For example, matrix alloying can be an effective approach to reducing coating degradation due to interdiffusion and reaction layer formation. The approach can be visualized in a number of ways. Alloying clearly influences the matrix activity and consequently reactivity with the reinforcement phase. Similarly, matrix alloying can also act to modify the diffusion path trajectory in a multiphase system [Bac 86]. In addition, matrix alloying can be used to some extent, to reduce the rate of interdiffusion by selective doping. Of course, the suitability of matrix alloying as a strategy for robust interfacial reaction kinetics control requires also a consideration of the influence of alloying on the mechanical properties of the matrix and the capability of the coating to tolerate a limited amount of reaction with the matrix without significant loss of strength and integrity.

During interdiffusion and reaction, composition gradients will continuously change and tend to decrease. Nevertheless, it is possible to design in gradients by appropriately adjusting the diffusion path through single-phase regions so that the gradients are maintained as the diffusion path settles into a steady state pattern as illustrated in Figure4 for a diffusion couple between pure A and the compound γ. For mass conservation the diffusion path outlined by the dotted line must pass through the line joining the end numbers of the couple [Kir 87].

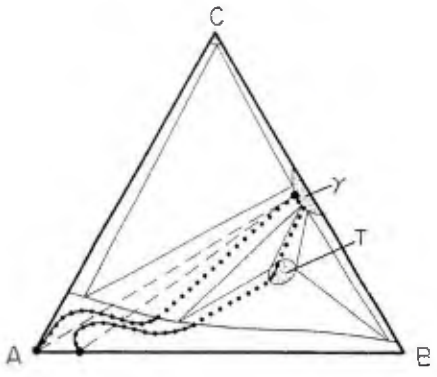

Figure 4: Illustration of the diffusion path (dotted curve) for a diffusion couple between the Al rich solid solution and γ phase. Changing the A rich solution composition modifies the diffusion path to include a ternary T phase.

For the case illustrated, component C is the most mobile component so that the diffusion path trajectory is directed toward the C corner of the isotherm. The path then recovers across the A-rich solid solution to seek out the tie-line between the A-rich solid solution and γ which is the stable steady-state path. Based on this information, the alloying of A with component B will alter the path to select other tie-lines between the A-rich solid solution and γ. Furthermore, the new tie-line can also link up with other phases in a ternary system such as the T phase, as shown in Figure4. Also, practically such concept can be extended to the interaction of oxygen with a multicomponent alloy such as that in the Ni-Al-O ternary system[McH 96]. In fact, carefully selected alloying and the introduction of composition gradients in the matrix can be useful methods for reaction layer selection and phase sequencing control. Moreover, the design of gradients of composition and phase structure can also provide a means of relaxing thermal cycle induced stresses as demonstrated by functionally gradient materials [Shi 93].

2.3 Diffusion Path Control and Kinetic Bias – Previous Studies

The synthesis of robust coatings that provide protection against environmental attack at ultrahigh temperatures is a difficult challenge. However, the current level of understanding does indicate that alloys in the Mo-Si-B system have sufficiently low inherent oxidation rates that a coating strategy can be used to realize the control that is needed to limit oxidation to satisfactory levels. The uncoated alloy substrate behavior during oxidation also highlights the substrate composition in terms of B/Si as a key element in coating design strategies. At the same time, it is evident that coatings will require integration with the substrate. In order to achieve compatibility upon integration, a multilayer coating structure is the most effective approach. In this way, structural compatibility will be assured as well as to provide a diffusion barrier to limit oxygen transport and to control the oxygen chemical potential. Often, in past work the approach to investigating multiplayer coatings has been a largely empirical one. However, in our past work, the use of the diffusion pathway and kinetic biasing concepts has been established as a fundamental method to analyze and to interpret multilayer coating reactions. Indeed, the lessons that can be

learned from the analysis and interpretation of the case study results provide the essential foundation for the proposed continuation of the research.

2.4 Diffusion Pathways and Oxidation Behavior of Mo-Si-B Substrate Alloys

In order to provide a baseline for comparison the development of oxide layer formation was analyzed in the uncoated alloy substrate. Ingots with a composition of Mo-14.2Si-9.6B (at%) were prepared by arc-melting in a Ti-gettered Ar atmosphere and sliced to 3 mm thick discs. For oxidation testing, an alumina boat containing the sample discs was inserted into a furnace at a preset temperature in air.

The Back Scattered Electron (BSE) image of an as-cast Mo-14.2Si-9.6B (at.%) sample and location of the composition on the ternary isotherm at 1600°C are shown in Figure5a and 5b. The as-cast microstructure is based on the Mo (ss) + T_2 two-phase eutectic and the finer three-phase eutectic structure (when the as-cast alloy is annealed at 1300°C for 100 hr the microstructure did not show a noticeable difference compared to the as-cast samples).

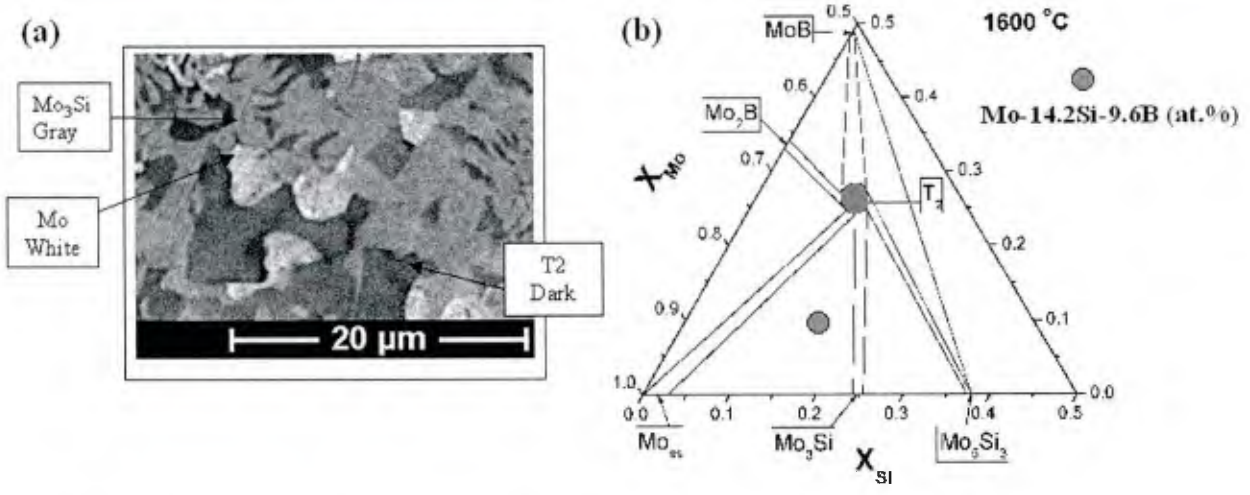

Figure 5. a) SEM Backscattered image of as-cast Mo-14.2at%Si-9.6at%B. b) Location of the nominal composition in the Mo-Si-B phase diagram.

The compositions of the oxide phases formed during exposure at 1000°C and 1200°C were quantified by EPMA (electron probe microanalysis). The amorphous layer was determined to contain mostly SiO_2 with about 10at.% B (or 17 mole% of B_2O_3) which is close to the liquidus at 1000°C [Mey 99] and in the MoO_2 layer the solubility of boron and silicon is negligible. From the layered product structure, the kinetic sequence involved in oxidation can be depicted in terms of the diffusion pathway that is represented in Figure 6a. The phase sequence in Figure 6b indicates that the borosilicate layer is connected to MoO_2 behind the initial pole between oxygen and the substrate composition. An examination of the pathway reveals that the composition of the borosilicate layer directs the initial phase development and influences the composition of the final product phases. For example, by enriching the SiO_2 content of the outer borosilicate layer, the equilibrium can be shifted from (borosilicate + MoO_2) to (SiO_2 + Mo) with a consequent drop in

the oxygen activity (i.e. Po_2) and the transport of oxygen to react with the alloy substrate. The absence of the MoO_2 layer signals a significant restriction on the oxygen activity ($Po_2 < 10^{-6}$ Pa) and flux.

Moreover, the viscosity of borosilicate solutions is significantly increased by the reduction of B to Si ratio. For example, when the B_2O_3 content decreases from about 17 to 12 mole %, the viscosity increases by an order of magnitude at 1200 °C [Ban 86]. The increase in viscosity in turn also decreases the oxygen diffusion rate [Ban 86]. It has been reported that the diffusion of oxygen in SiO_2 layer can occur by two main modes: molecular permeation and network oxygen self diffusion . From the oxide thicknesses and the oxidation times, the estimated oxygen diffusivity is in the range of 10^{-15} to 10^{-17} m^2/sec, which is comparable to the values for network oxygen diffusion and several orders of magnitude slower than the values for molecular permeation of oxygen. This also indicates that oxygen diffusion governs the oxidation process [Lam 92].

To further modify the oxidation behavior of Mo-Si-B alloys, a pack cementation coating of silicon was utilized. This process produces molybdenum silicides on the surface of the material, and when exposed to oxygen, these will form a protective layer of SiO_2. The nominal thickness of the $MoSi_2$ layer was observed as about 10 μm. During the Si pack cementation process, the inward Si diffusion [Mue 92, Coc 95, Par 02a] to the substrate results in the formation of mainly the $MoSi_2$ phase. Also, silicon, instead of molybdenum, mainly contributes to the formation of $MoSi_2$ and other silicides, which is consistent with the pack cementation observation (i.e. inward diffusion of Si [Mue 92, Coc 95, Par 02a].

Silicon is the main diffusing element into the substrate during the pack cementation process, resulting in the formation of the $MoSi_2$ outer layer. However, the $MoSi_2$ phase is in equilibrium with the MoB and T_1 phases in the ternary Mo-Si-B system (see Figure 1), which is different than the phase combination of the as-cast alloy composed of Mo, Mo_3Si and T_2. In fact, TEM evaluation clearly reveals the presence of MoB particles within the $MoSi_2$.

Upon oxidation testing of the current silicide coated samples, a thin oxide layer formed at outer layer, similar to the previous results [Kir 92]. The observed typical thickness of the scale after the oxidation test at 1200°C for 100 hours was less than 5 μm. Upon oxidation at 1200°C, the synthesized $MoSi_2$ phase has completely transformed into Mo_5Si_3 (T_1), when the exposure time reached 50 hr. With further oxidation exposure up to 100 hours at 1200°C, the T_1 phase coating appears to remain stable and retain an excellent oxidation resistance. From this perspective, the use of a $MoSi_2$ and Mo_5Si_3 (T_1) phase coating appears to be effective in inhibiting the oxygen penetration to the substrate and furthermore remains intact with the substrate. Moreover, the transformation of the $MoSi_2$ coating layer into Mo_5Si_3 (on the substrate side) and SiO_2 (on the free surface of $MoSi_2$ coating layer) as well, indicates that silicon depletion is a significant factor for determining the molybdenum disilicide coating lifetime [Coc 95]. Moreover, the boron-doped Mo_5Si_3 (T_1) thin layer exhibits a superb high temperature oxidation resistance [Mey 96].

The diffusion pathways with the silicide coatings have been depicted in Figure 6, which shows that the coating eliminates the formation of both the internal oxides (layer no.1) and the MoO_2 (layer no. 2) as a consequence of a much lower oxygen partial pressure within the coating.

It is also worth noticing that the thickness of the Mo_5Si_3 phase for the current experiments does not show a considerable thickness change even after a complete elimination of the $MoSi_2$ phase. This implies that there must be an effective diffusion barrier formed underneath the T_1 phase coating inhibiting Si diffusion into the substrate and consumption of T_1. In fact, it has been established that the diffusivity of Si in the T_2 phase is 10^3 times slower than in the T_1 phase and thus, the T_2 phase serves as an effective diffusion barrier.

Since the outer borosilicate layer growth upon high temperature exposure for the coated sample is not significant, the main reservoir for the Si content in the shrinking $MoSi_2$ layer should be the substrate. The T_2 layer (beneath T_1 layer) together with Mo_3Si exists and both phases protrude into the substrate. As expected, upon Si inward diffusion mainly the Mo phase is transformed into the Mo_3Si and the T_2 phases. From the observations of the oxidized pack cementation sample and recalling that the substrate is composed of two eutectics (Mo + T_2 and Mo_3Si+T_2), the resultant reaction for the formation of T_1 (Mo_5Si_3) and T_2 (Mo_5SiB_2) may be written:

$$Mo(ss) + T_2 \rightarrow Mo_3Si + T_2 \rightarrow T_1 + T_2 \quad (2.4)$$

$$Mo_3Si + T_2 \rightarrow T_1 + T_2 \quad (2.5)$$

The reactions and the resultant coating phase evolution can be understood based upon the diffusion pathway depicted in Figure 6.

It should be stressed that the identification of product phases can be inversely applied as a guideline for operating conditions. In fact, the identification of the MoO_2 formation in this oxidation procedure provides a guideline for estimating the maximum oxygen partial pressure for the MoO_2 formation. For this purpose, it is useful to examine the oxygen partial pressure-species diagram for molybdenum oxidation as shown in Figure7a [Gul 79]. The solid lines are from the calculation at 1250K (977°C) and the dotted vertical lines indicate the boundaries at 1200°C. In principle, the increment of temperature only increases the equilibrium oxygen partial pressure and does not change the slopes of oxides equilibrium lines, indicating that temperature variation does not change the dominating species, but affects equilibrium partial pressure. The vertical lines of the diagram section the stable phase areas – Mo, MoO_2(s) and MoO_3(l).

In the oxidation of Mo-Si-B alloys initially MoO_3 forms preferentially, but this layer offers no protection to continued oxidation. The high pressure of $(MoO_3)_3$(g) indicates that $(MoO_3)_3$ is the most volatile species in the range of between 10^{-12} to 1 (atm) oxygen pressure, indicating that this may lead to a considerable loss of material without any protective layer above 1250K. The maximum oxygen maximum pressure for MoO_2 formation is estimated about 10^{-7}atm at 1000°C and 10^{-5} atm at 1200°C. For SiO_2 and B_2O_3, similar oxygen partial pressure diagrams are available [Gul 79, Sin 91], as shown in Figure 7b and Figure 7c, respectively.

The dominating species based upon equilibrium oxygen vapor pressure indicates SiO_2(g) and B_2O_3 (g) at lower oxygen partial pressure (in air). While such a thermodynamic approach cannot quantify the extent of species volatilization, it can provide a basic guideline for predicting possible reactions. For example, in the Mo-Si-B ternary alloy system, MoO_3 (g), SiO_2(g) and B_2O_3

(g) are possible volatile species at high temperature. The initially formed MoO_3 layer can be transient because it sublimates readily at temperatures above 700°C to leave a surface that is enriched in Si and B. The enriched surface then develops a protective SiO_2 layer that also contains B_2O_3 and provides a reduced oxygen activity so that MoO_2 forms at the base alloy surface. Moreover, it has been documented that at temperatures between 1100K and 2300K boron loss can occur due to evaporation [Sin 91].

Several oxidation studies have been done using thermogravimetric analysis to examine the behavior of Mo-Si-B alloys over longer periods of time. One study by Yoshima focused on the T_2 composition (Mo-12.5Si-25Bat.%, B/Si = 2) and involved testing the alloy at temperatures between 700°C and 1400°C for up to 24 hrs [Yos 02]. At low temperatures, the alloy initially gained mass, but then started to lose mass as MoO_3 began to evaporate at a significant rate. At all temperatures higher than 1000°C, the alloy lost some mass continuously during the test, indicating that molybdenum is being oxidized and is evaporating concurrently with the oxidation of silicon and boron. This indicates that while the scale that formed on the sample was somewhat protective, it did not reduce the partial pressure of oxygen to the point where molybdenum would not oxidize. This means that the oxygen transport through the scale was appreciable, and that it is too rich in boron oxide.

Mendiratta et al. [Men 02] tested six different Mo-Si-B alloy compositions in a cyclic oxidation environment that cycled from 1200°C to room temperature to determine behavior as a function of B/Si. The Mo-11Si-11B (at%) alloy performed best in this type of test, showing a very small mass change over 100 hrs of testing. Alloys that did not perform well tended to have high levels of boron and lower levels of silicon. It was also found that none of the alloys were passivated at lower temperatures, and all suffered from catastrophic oxidation (i.e. pesting) between 700°C and 800°C. Bubbles were observed in the Mo-11Si-11B alloy scale at 800°C, indicating that oxidation of molybdenum was occurring and that the MoO_3 bubbles were moving through the scale. This behavior illustrates the ease with which material may be transported across the protective scale if the chemistry is not optimized.

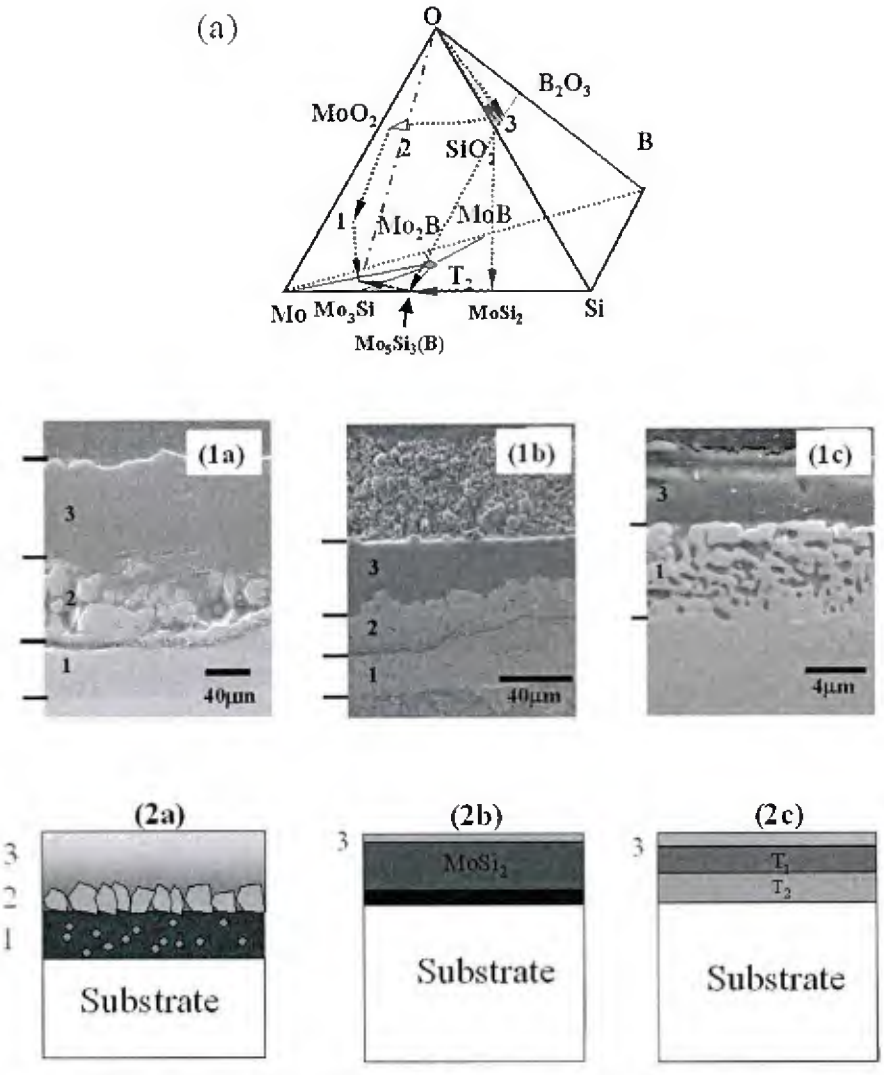

Figure 6: (a) Schematic illustration of the diffusion pathway indicating the phase evolution upon oxidation of a Mo-Si-B alloy located in the Mo-Mo_3Si-T_2 three phase field (virtual diffusion path between borosilicate and MoO_2 is also indicated). (The numbers indicate (1) Mo(ss) phase with internal oxide precipitates, (2) MoO_2 and (3) borosilicate layer. The region below (1) in (a) is the alloy substrate.) The diffusion pathway can be further modifies by Si surface enrichment which yields $MoSi_2$ or B-doped Mo_5Si_3 oxidation resistance coating layers. Note that with this approach path no.1 (internal oxides) & 2 (MoO_2) can be eliminated. (1a) Cross section BSE image of the Mo-14.2Si-9.6B (at.%) alloy oxidized at 1200°C for 100 hr in air. (1b) Cross section BSE image of crystal SiO_2 powder. (1c) Cross section BSE image of amorphous SiO_2 powder sprayed Mo-14.2Si-9.6B (at.%) alloy following oxidation at 1200°C for 100 hr. (2a) Schematics of diffusion pathways in Uncoated Mo-Si-B substrate (2b) Si-pack Mo-Si-B (2c) Si-pack Mo-Si-B after prolonged exposure. As shown in (2b) and (2c), layers #1 and #2 do not develop, instead only the borosilicate layer forms (layer #3). Both (2b) and (2c) show excellent oxidation resistance due to the disilicide (in 2b) and or T_1 + T_2 phases (in 2c).

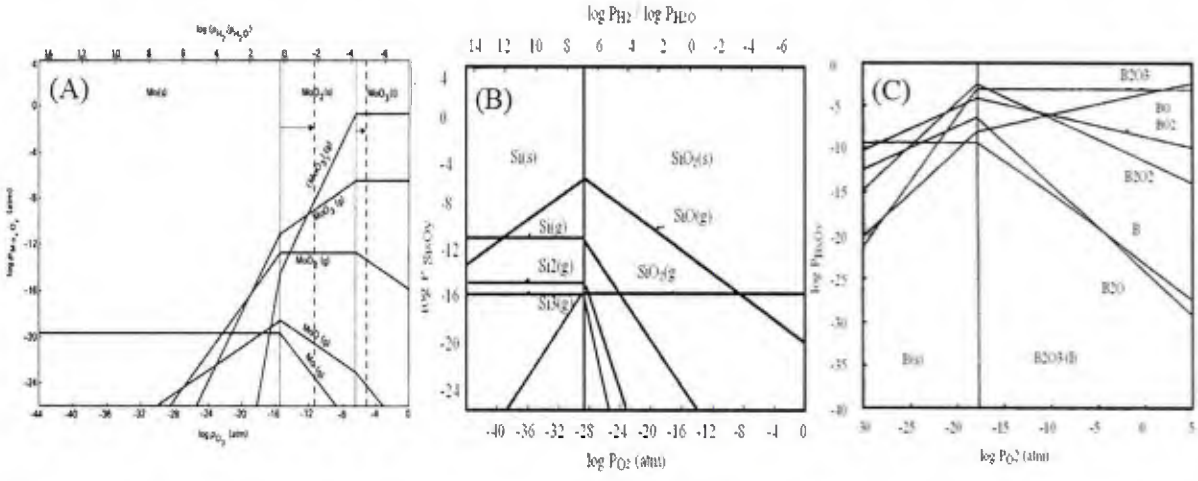

Figure 7. a) Equilibrium vapor pressure (log P) of different species of the Mo-O system as a function of oxygen partial pressures at 1200°C. b) Equilibrium vapor pressure (log P) of different species of the Si-O system as a function of oxygen partial pressures at 1250K (977°C) [Gul 79]. c) Equilibrium vapor pressure (log P) of different species of the B-O system as a function of oxygen partial pressures at 1700K (1427°C) [Sin 91].

From the reported observations, the general features appear to be that in all cases there is a transient stage which is accompanied by mass loss due to the evaporation of MoO_3 as well as boron oxide. The oxidation process then proceeds with the eventual formation of a steady state which is signified by the development of borosilicate layer at the outermost portion of the oxide structure. The SiO_2 ($+B_2O_3$) layer produced is naturally protective, but it does not completely block O_2 transport so that with continued exposure, the thickness of the oxide increases along with a recession of the alloy base. The initial onset temperature for the steady state oxidation is highly dependent the composition of the Mo-Si-B substrate alloys. Furthermore, the B/Si ratio in the substrate and that develops in the oxide scale controls the nature of the transient stage. The significance of the B/Si ratio opens up opportunities in coating design to alter the oxygen diffusion pathways and consequently the overall oxidation resistance as elaborated in the next section.

2.5 Mo-Si-B Based Coatings

From the current observations as well as from prior reports, the oxidation reaction commences with a transient stage which is accompanied by mass loss due to the evaporation of MoO_3 and boron oxide. The oxidation process then evolves into a steady state which is signified by the development of borosilica layer at the outermost portion of the oxide structure. Following oxidation in air the SiO_2 ($+B_2O_3$) layer produced is naturally protective, but it does not completely block O_2 transport so that with continued exposure, the thickness of the oxide increases along with a recession of the alloy base. The onset temperature for the steady state oxidation is highly dependent the composition of the Mo-Si-B alloys. Furthermore, the B/Si ratio in the substrate and that develops into the oxide scale controls the nature of the transient stage. The significance of the

B/Si ratio opens up opportunities in coating design to alter the oxygen diffusion pathways, the oxygen mobility and consequently the overall oxidation resistance.

In order to control the B/Si ratio a pack cementation process was adapted for coating synthesis. During the silicon pack cementation process coating process, a steep chemical potential gradient of Si across the vapor-substrate interface produces a flux of Si into the substrate that uniformly enriches the local Si concentration and results in the synthesis of a $MoSi_2$ coating layer [Lev 74, Mue 92, Coc 95]. A BSE image of an as-Si packed sample is shown in Figure 8a. Underneath the $MoSi_2$ layer, there is a Mo-rich silicide layer of Mo_5Si_3 (T_1) phase and dispersoids of the MoB phase [Sak 05]. There is a limited amount of boron in the substrate and consequently it is not possible to establish a continuous layer of MoB.

The presence of MoB phase can be understood from the diagram of composition trajectories of the Si-pack cementation process into this alloy as shown in Figure 8b. In this case, due to the relatively low temperature of the pack process (900°C), any preferential mass loss of the elements (Mo, Si, B) on the surface due to evaporation should be negligible. Thus, as Si diffuses into the Mo-Si-B alloy, the composition trajectory should follow the line connecting the Si source to the composition of the substrate (Mo-3Si-1B wt.%, Mo-8.9Si-7.1B at.%). From the tie line between MoB and $MoSi_2$ in the Figure 9b, it is clear that only a limited amount of MoB (as the boron source) that can be created as the $MoSi_2$ layer starts to develop on the surface.

Enrichment of silicon via pack cementation does not provide the amount of boron needed to stabilize a continuous layer of borosilicide and/or boride phases. Therefore, it is important to pursue a simultaneous or co-deposition of B and Si onto the Mo-rich Mo-Si-B alloys followed by annealing treatments at 1200–1400°C [Per 08, Per 06]. Indeed, as exemplified in Figure 9a, by partly substituting Si with B in the pack powder mixture, a continuous layer of MoB can be stabilized underneath the silicide layer coating onto the Mo-3Si-1B wt% substrate. As illustrated in Figure 9b, the nominal composition path for the co-deposition processes can be represented by rotation about the substrate nominal composition whereby the initial vapor source moves from the pure Si to a mixed Si/B source.

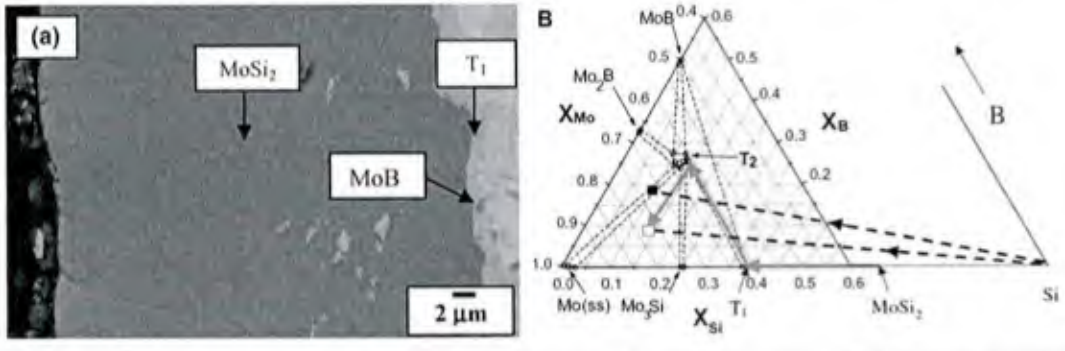

Figure 8. a) Si Pack-cementated Mo-3Si-1B (wt %) b) Composition trajectory of Si+B pack cementation process on Mo-3Si-1B (wt %) alloys depicted in the Mo-Si-B phase diagram.

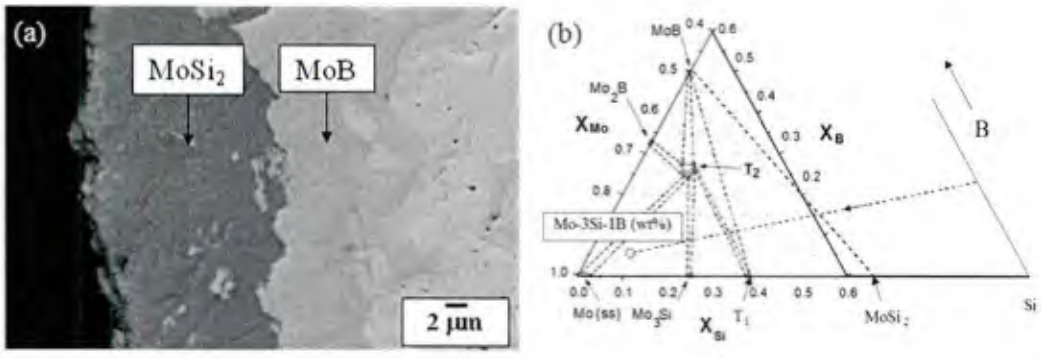

Figure 9. a) Pack-cementated Mo-3Si-1B (wt %) with a partial substitution of Si with B (1:20 B to Si weight ratio) b) Composition trajectory of Si+B pack cementation process on Mo-3Si-1B (wt %) alloys depicted in the Mo-Si-B phase diagram. A full development of the boride phase underneath the silicide phase is observed with the partial substitution.

During oxidation tests of the (B+Si)-pack alloys, the initial $MoSi_2$ outer layer is consumed by formation of the T_1 phase as one consequence of the transient composition trajectory. With continued elevated temperature exposure during oxidation, the outer T_1 phase layer would eventually be consumed by dissolution into the substrate. However, part of the initial transient stage of reaction that yields the T_1 phase from the inward flux of Si and B also leads to the development of the T_2 borosilicide and/or boride phase layer. The relative amounts of the T_2 and MoB phases below the T_1 phase region depend on the B/Si ratio of the powder sources as illustrated in the diffusion path trajectory in Figure 9b. The T_1 phase is always in contact with the MoB or T_2 borosilicide phase, which guarantees B saturation in the T_1 phase. Furthermore, since the T_1 phase that is saturated with B has excellent oxidation resistance [Mey 99] and the loss of Si is blocked by the underlying diffusion barrier (i.e. the borosilicide and boride phases), the T_1 layer thickness change can be arrested [Per 08, Per 06]. Further, any damage to the outer T_1 layer can be recovered from the underlying T_2 + MoB layer. In effect, the in-situ reaction that yields the T_2 + MoB layer also provides a kinetic bias [Per 95] that allows for the continued existence of the outer T_1 layer and also yields a self-healing characteristic of the coating and resistance to pesting.

Oxidation tests performed at 1400°C show the benefits of the coatings to provide an effective oxidation protection. As shown in Figure 10a and 10b, with uncoated samples, oxidation of Mo-3Si-1B (wt. %) alloys results in a large mass loss as evident by the thick borosilica glass and intermediate region depleted in Si and B. The SEM cross section of the oxide scales shows that even though there is a thick and continuous borosilicate layer on the surface, the high evaporation rate of B_2O_3 at this temperature results in a relatively large mass loss during the transient oxidation. In contrast, the coated sample in Figure 10c and 10d shows the thickness retention of the sample and furthermore a very limited growth of the borosilicate layer on top of the coating (less than 15 µm after 30 hrs exposure).

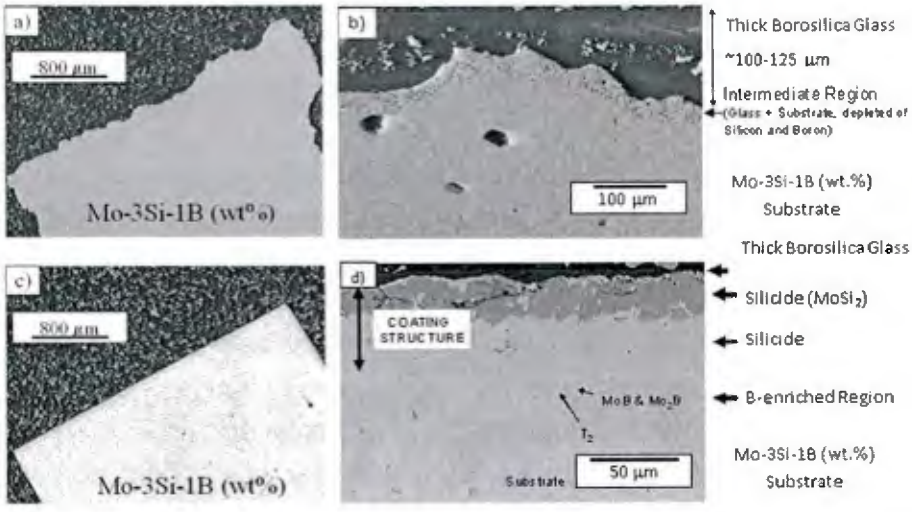

Figure 10. SEM image of uncoated Mo-Si-B sample after an oxidation test at 1400°C for 10 hours showing the extensive recession rate even though a continuous borosilica layer develop on the surface as shown in back-scattered SEM image in (b). In contrast, with the same oxidation condition the coated sample in (c) exhibits a minimal mass loss due to the borosilicide coating protection. (d) SEM back-scattered cross-section image of the coating showing the development of B-saturated T_1 and the diffusion barrier underneath comprised of the T_2 and boride phases.

3. Current Studies

A clear understanding of the factors controlling reproducible and robust coating synthesis and processing is critical for high temperature applications. Coatings usually behave as interfacial materials since their processing and performance are dominated by the characteristics of interfaces. In order to achieve stable, in-situ multiphase designs, the principles governing the controlling interface reactions are being examined at a basic level. In fact, the understanding of interface reaction control has a wide application in a number of advanced materials systems such as those involved in coatings for oxidation protection and thermal barrier functions.

In the current program, the key objective is to capitalize on the interdiffusion reactions between potential materials combinations to develop useful reaction products and alloy compositions that evolve toward a steady state of a compatible system. The operating principles of interface reactions in multicomponent systems are being examined at a basic level to develop design strategies, which will provide useful guidelines for developing stable and robust composite and coating systems. As part of this goal, a kinetic bias concept which has been demonstrated to be effective in modifying interface reaction products, controlling the reaction product phase sequence and even in controlling porosity during interface reactions is also being examined further for coating applications where multiple functional layers coexist. In order to achieve compatible interfaces to maximize the high temperature stability and performance, key issues such as identifying oxidation steps, recession rate and coating compatibility must be considered for an effective coating strategy development.

In applying these guiding principles in the current work, we have focused on a number of aspects critical to the coating performance and application, namely (1) The capability of MoSiB coatings to suppress hot corrosion attack, (2) The oxidation resistance of MoSiB coatings in a water vapor environment (3) The extended use of MoSiB coatings for environmental protection of SiC/C Composites and (4) The influence of minor alloying additions on the oxidation response of Mo-Si-B alloys. We have made significant progress in adapting the MoSiB-based coating design to provide extended functionality on a variety of metallic and ceramic substrates, have identified a methodology to scale up the coating application for commercial use and have developed a mechanistic understanding of some parts of the coating performance. In order to build on this progress and advances in the fundamental understanding we propose a continuing study with a focus on (1) Developing a fundamental understanding of the MoSiB coating structure and the influence of additives that is the basis for the remarkable effectiveness, (2) Establishing the long term stability of the coating effectiveness (along with a lifetime model) during high temperature isothermal and thermal cycling exposure, (3) Examination of the coating performance in other environments such as low oxygen partial pressures and high velocity steam conditions and (4) Continuing the study of MoSiB based coatings for environmental protection of other refractory metal alloys and high temperature materials.

The advances in understanding during the current program have provided the essential foundation to address the key issues regarding alloy composition and microstructure, enhanced coating protection, thermal cycling behavior and lifetime modeling. These developments are highlighted in the following discussion. The discussion covers selected areas from the current work that provide a perspective on the efforts that are proposed to advance the understanding and application of coatings to the next level.

3.1 Mo-Si-B Coating Resistance to Magnesium Sulfate based Hot Corrosion

A variety of salt deposits from fuel impurities and the atmosphere have been found in turbine engines [Bor 97]. The degradation of materials by these salts at the operational temperatures of turbines is defined as hot corrosion [Eli 02]. Hot corrosion is the accelerated corrosion of a material when salt deposits melt and damage the protective surface oxides. Previous studies have investigated the Mo-Si-B coating resistance to calcia-magnesia-aluminosilica [Dow 14] and sodium sulfate (Na_2SO_4)/sodium vanadate (Na_3VO_4) [Tay 17]. The present study investigates the protective ability of the coating in ($MgSO_4$) environments.

Constituent	Composition (wt %)	Composition (mole %)
Na_2SO_4	56.5	54.68
K_2SO_4	6.97	5.5
$CaSO_4$	14.85	15
$MgSO_4$	21.73	24.82

Table 1 Table of recorded salt presence in turbine engines by Bornstein and Allen

Magnesium sulfate comprises 22% of the salt deposits found in turbines [Bor 97]. Both $MgSO_4$ and Na_2SO_4 have similar decomposition routes producing SO_3 and an oxide [Sch 11,Law 90]. It has been shown that sodium oxide (Na_2O) diffuses into the outer vitreous silica layer of the Mo-Si-B coating promoting the nucleation of cristobalite [Tay 17]. This crystallization front advances into the silica and causes some loss of the coating from spallation. In contrast, magnesium has virtually no mobility in silica [Muk 02]. Due to this, magnesium forms less cristobalite and maintains a larger amount of vitreous silica, preserving the Mo-Si-B coating. The liquidus projection in Figure 11 of MgO, Na_2O, and SiO_2 highlights this strong inactivity of magnesium oxide which is stable over a rather large composition range in this system. This diagram was adapted from the FactSage program [Bel 10].

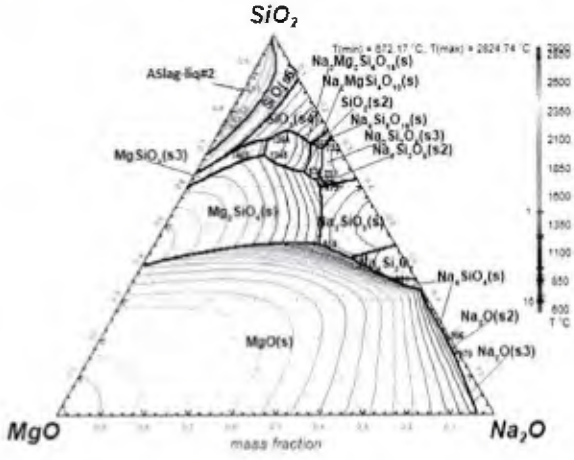

Figure 11 Liquidus projection of MgO, SiO2, Na2O from the Factsage program

The temperature of salt decomposition is a contributing factor to the severity of the corrosion. The relation of free energy to temperature of the decomposition of various sulfates to sulfur dioxide and sulfur trioxide was calculated using standard thermodynamic values [Lid 03, Dea 79]. Sulfur dioxide is the more favorable decomposition with $MgSO_4$ decomposing at 640°C, $CaSO_4$ decomposing at 916°C, and Na_2SO_4 at 1355°C. Figure 12 presents this data where it can be seen that both magnesium and calcium sulfate begin to decompose to sulfur dioxide at or below the Type 1 corrosion temperature threshold of 825°C [Str 98]. Some of the decomposing $MgSO_4$ reacts with MoO_3 to form $MgMoO_4$, but most of it is assumed to form inert MgO that remains solid on the surface to later fall off when the sample is removed according to the reactions in equations 1 and 2. This low temperature decomposition causes these sulfates to leave the system, limiting the amount of corrosion they can cause. Sodium sulfate decomposes at far higher temperatures allowing it to remain a source of corrosion during the entirety of turbine operation.

$$MgSO_4 \rightarrow MgO + \frac{1}{2}O_2 + SO_2 \quad (1)$$

$$MgO + MoO_3 \rightarrow MgMoO_4 \quad (2)$$

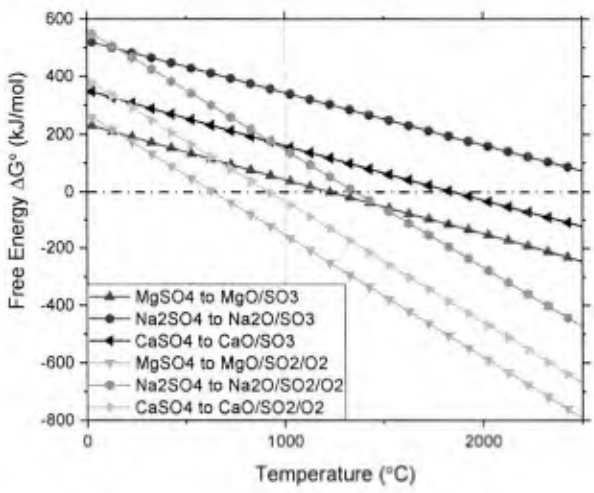

Figure 12 Temperature free energy relation of the decomposition of various sulfates

Experimental procedure

The effects of these salt systems on Mo-Si-B coatings were explored by producing a series of coated molybdenum coins that were exposed to hot corrosion environments. Pure molybdenum (99.95%) rods were cut into coins approximately 1.25 cm in diameter and .3 cm thick. A coating from a source of Si and B in the ratio of 35:1 silicon to boron was deposited via pack cementation in a powder mixture and heated in an argon filled tube furnace at 1000°C for 50 hours. The powder mixture contained 2.5 wt% NaF salt as an activator, 35 wt% of a 35:1 silicon to boron powder and 62.5 wt% of inert alumina.

After the pack cementation, the coins were conditioned in laboratory air at 1300°C for 10 hours. This conditioning served two functions. Primarily, it oxidized the surface forming the vitreous outer layer [Rio 09]. Secondly, it verified the integrity and completeness of the coating. If the coating was incomplete, the molybdenum substrate would rapidly oxidize to molybdenum trioxide (MoO_3) and vaporize. This failure of the coating was visually apparent and caused a significant mass loss allowing for easy detection.

The conditioned coins were coated in a salt solution as an analog to salt deposition in turbines. A slurry of magnesium sulfate or the composite salts was applied to the coins using an airbrush. The amount of salt applied was approximately 25 mg/cm^2 for the magnesium system and 10 mg/cm^2 for the composite system. This amount is several orders of magnitude beyond reported salt amounts to promote corrosive effects [Ash 69]. The composite salt slurry was a mixture of salts found in existing jet engines, along with environmental salts, and elements related to fuel impurities [Bor 97,Bor 93]. The final constituents are presented in Table 2. The coated specimens were dried in open air until the salt slurry densified. Vapor phase mass loss experiments using a salt reservoir were not attempted as it has been shown to have significantly lower mass losses [Tay 17].

The coated coins were loaded into a tube furnace. In the furnace the coins were exposed to repeated thermal cycling of 5-hour periods at either 900°C or 1000°C. During the cycles the air

Ion	Na	V	SO_4	Mg	Ca	Cl	K
Approximate Molar Percent	38	4.5	27	11	7.5	10	2
Salt Species	Na_2SO_4	$NaVO_3$	$MgSO_4$	$CaCl_2$	KCl		
Approximate Molar Percent	41	20	21	14	4		

Table 2 Molar percentages of each ion present in composite salt slurry

was either left static in the furnace or laboratory air was flowed over the coins at a rate of approximately 10 l/min. The large quantities of salt and relatively slow air speeds make the conditions tested far more favorable for hot corrosion attack than turbine operation. After each cycle the mass of the coin was measured, and x-ray diffraction was performed periodically. The salt coating was not reapplied during the cycles as Sumner et al. have shown that redeposition has little effect on corrosion for the time scales used here [Sum 17]. Select coins were sectioned and polished for scanning electron microscopy. Before sectioning the coins were coated with a sputtered gold and an electroplated nickel layer to preserve the glassy silica coating during the polishing according to a procedure outlined by Richter [Ric 12].

Results

The mass loss of the coins after each cycle is presented in Figure 13. There is an initial gain in mass from the salt coating. After this gain the coating stabilizes and the total mass change plateaus to near the initial mass before the salt coating application. Coins that were in a flowing air environment showed a stable mass change closer to the zero, likely due to the air physically removing salt deposits on the surface. The 1000°C cycles in the static environment showed some mass loss similar to sodium environments, but to a lesser extent. This is at the temperature where the $MgSO_4$ decomposes which could contribute to the increased severity of the attack. The 900°C static salt environment did not have a net mass loss as some amount of salt remained on the surface throughout the experiment. These results show a clear difference with the sodium sulfate (Na_2SO_4)/sodium vanadate (Na_3VO_4) mass loss as shown in Figure 14. In most cases there is significantly less mass loss in the $MgSO_4$ coated samples than those coated with $Na_2SO_4/NaVO_3$. The mass loss for both magnesium and $Na_2SO_4/NaVO_3$ was similar only for the 900°C flowing air environment, which was relatively inactive for both.

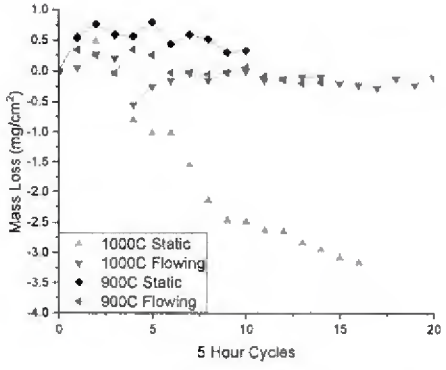

Figure 13 Mass loss of Mo-Si-B coins in different magnesium sulfate environments

The consistent reduction in mass loss can be attributed to the lack of magnesium mobility in the silica. In static environments the mass loss during $MgSO_4$ exposure is consistently $1/10^{th}$ of the Na_2SO_4-based mass loss. The mass change in flowing air environments were more temperature dependent. At 900°C the $MgSO_4$ corrosion was $1/5^{th}$ that due to $Na_2SO_4/NaVO_3$, whereas at 1000°C the corrosion was $1/20^{th}$ a result of increased reactivity in the $Na_2SO_4/NaVO_3$ system at higher temperatures. Since the magnesium does not move through the silica advancing a crystallization front, large cristobalite regions do not form and subsequently spall off, as described in the $Na_2SO_4/NaVO_3$ environments [Tay 17,Muk 02]. Additionally, a sample was tested at 1300°C in a static environment. The mass loss of this sample stabilized at -3 mg/cm^2, comparable to the mass loss in the 1000°C static environment. .

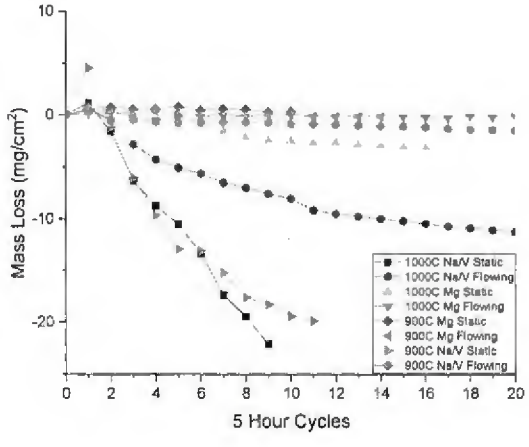

Figure 14 mass loss data of Mo-Si-B coated coins in both magnesium sulfate and sodium sulfate (Na_2SO_4)/sodium vanadate (Na_3VO_4) environments.

X-ray Diffraction was used to identify the composition and structure of the Mo-Si-B coatings after the conditioning and during the thermal cycles. The majority of the coating is the expected vitreous borosilica layer that appears as a broad amorphous region in x-ray diffraction.

In addition, multiple series of peaks associated with the molybdenum silicon structures of T_1 and $MoSi_2$ are clearly detected. Some regions of the coins showed peaks consistent with magnesium molybdate ($MgMoO_4$) as shown in Figure 15.

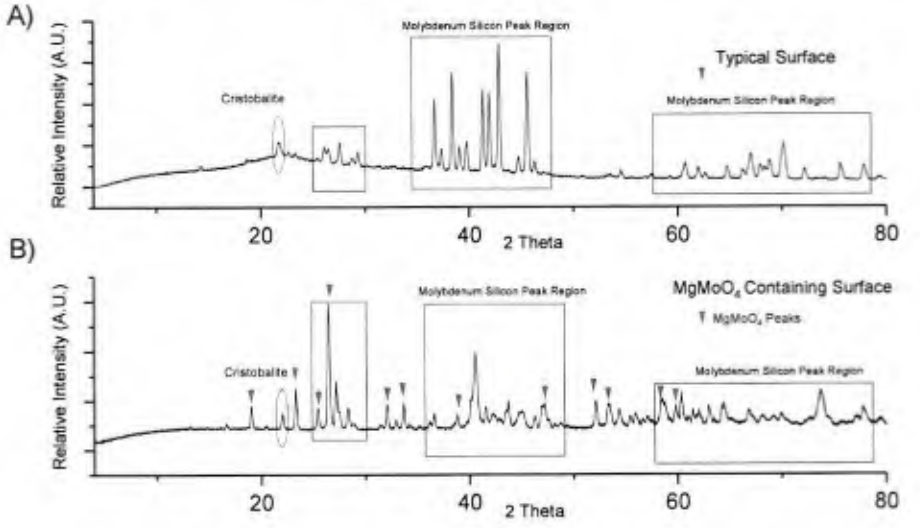

Figure 15 X-ray diffraction of A) a typical region of Mo-Si-B coated coin surface after magnesium sulfate exposure and B) regions containing MgMoO4 after 20 5 hour cycles

The formation of $MgMoO_4$ is thermodynamically favored in the presence of MgO and MoO_3 as demonstrated in Figure 16 where there is a thermodynamically favored region above 600°C where $MgSO_4$ decomposes to MgO which reacts with MoO_3 or Mo and O_2 to form $MgMoO_4$. The relative scarcity of $MgMoO_4$ and the lack of noticeable mass change implies that it is not the result of a breach in the coating but a reaction of molybdenum still present in the surface layers after the pack cementation process.

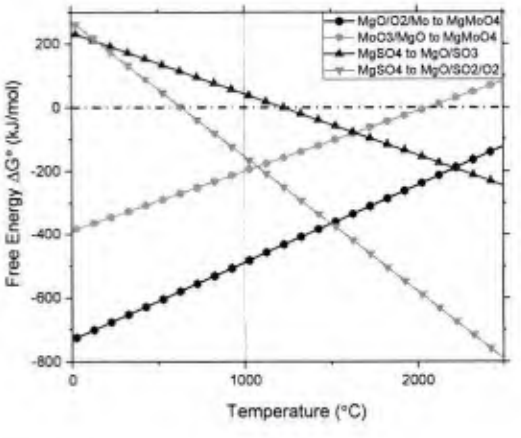

Figure 16 Temperature related free energy of the decomposition of $MgSO_4$ and the formation of $MgMoO_4$

The SEM image in Figure 17 shows cracks where silica has flowed into gaps in the coating. These gaps are a probable source of the molybdenum that oxidizes to MoO_3 which reacts with MgO to form magnesium molybdate. In order to assess the self-healing capability of the coating system it is necessary to consider the flow velocity of silica. The works of Papko and Levitskii, and Saiz et al. provide the foundation to approximate the self-healing rate [Lev 11,Sai 07]. Papko and Levitskii found the viscosity, η of a 70% silica glass at 900°C, with other oxides including B_2O_3 accounting for no more than 10% each, to be $10^{5.2}$ Pas·sec. Saiz et al. found the spreading velocity, v of a silica glass on molybdenum at 1200°C to be approximately 90 $\mu m \cdot sec^{-1}$ and related to the Capillary number, $C_a = \eta v/\gamma_{lv}$. Using their capillary number of $9 \cdot 10^{-2}$ and an interfacial tension, γ_{lv} of ~1 $J \cdot m^{-1}$ an approximate viscosity of 10^5 Pas·sec can be calculated. From these values an overestimated spreading velocity of 90 $\mu m \cdot sec^{-1}$ can be used. Using this, cracks such as A and B in Figure 17 could be filled in less than 10 seconds at 1000°C.

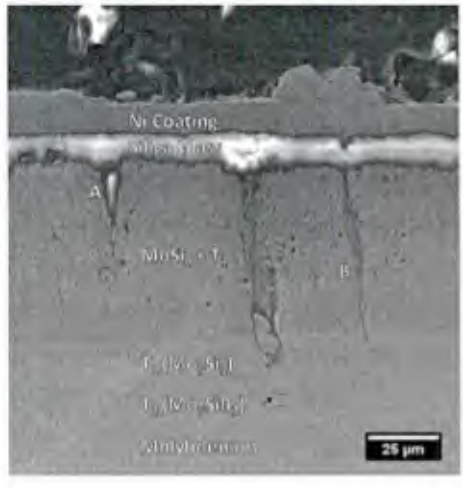

Figure 17 SE - SEM image of cracks in the surface coating that have been filled in by silica during thermal cycling

Conclusion

Magnesium, which appears in turbine engines via magnesium sulfate in isolation has little detrimental effect on Mo-Si-B coatings for refractory metals in normal operating conditions. Unlike sodium there is little crystallization of the outer vitreous silica layer except in extreme 1000°C static thermal cycling environments. Examinations of the mass changes during repeated thermal cycles and changes in the x-ray diffraction of the surface support this. It was noted that magnesium molybdate does form on the surface of some coatings as a reaction of the decomposing magnesium sulfate and molybdenum.

Repeated thermal cycling the composite salt mixture of Na_2SO_4, $NaVO_3$, $MgSO_4$, $CaCl_2$, KCl, demonstrated a consistent level of impact on the silica coating. Following an initial period of corrosion and mass loss the silica coating stabilizes. This mass loss remained at or less than 2 mg/cm^2 for all tested environments including a composite salt mixture. After investigating the composite salt mixture isolated sodium salts remain the most deleterious to the silica coatings but did not induce failures exposing the molybdenum core to oxygen. Against the range of salts and

impurities that occur in turbine engines under normal operations silica coatings derived from Mo-Si-B systems demonstrate significant and reliable resilience.

3.2 SEM and Raman spectroscopy studies on Si-B pack cementation followed by Al coatings and wet oxidation behavior

For the examination of the constitution and structure of the MoSiB based coating three conditions were analyzed by SEM/EDS and Raman Spectroscopy. The treatments included the Si and B codeposition by pack cementation on a Mo substrate and the subsequent addition of Al to the pack cementation coating

Experimental details

The pack cementation treatment with a 35:1 Si and B mixture was done on Mo substrate at 1000 °C for 50 h in argon environment and then conditioning was carried out at 1300 °C for 2 h in air. After finishing the coatings and conditionings, wet oxidation experiments were carried out at 1450 °C for 35, 40 and 75 h in air. For each treatment step, scanning electron microscopy (LEO-Inspect F) equipped with energy dispersive spectroscopy (EDS), and X-ray mapping were used to identify surface morphology and elemental distribution on top of the surfaces. The Raman spectroscopy (Model: Horiba Labram Aramis, He-Ne laser with 532 nm, laser spot size of 1 μm, acquisition time: 5min, grating 1800, with D1filter at 100 x) was done on the wet oxidized samples to identify the polymorphs of SiO_2 and oxide products.

Results and Discussion

SEM/EDS mapping of Si-B pack cementation

SEM and EDS analysis of Si-B pack cementation sample at 1000 °C for 50 h in argon environment revealed both light and dark regions on the top surface of the pack coating. The Na, O and Al elements are enriched in the dark regions and Si and Mo elements are richer in the light regions which represent the Mo_5Si_3 (T1) and $MoSi_2$ phases that form during pack cementation. Following Si-B pack cementation conditioning at 1300 °C for 2 h in air the analysis demonstrated that Al and Si elements are enriched in the light regions whereas Mo is enriched in the dark regions. It was also observed that oxygen is uniformly distributed throughout the surface. After conditioning, some amount of Na still appears on the coating surface, but a significant amount of Al was not detected on the conditioned sample.

While these results are preliminary they do suggest some characteristics in the coating evolution. First, since the coating appears to be glassy macroscopically the detection of Mo probably comes from the T_1 and $MoSi_2$ phases under the glass due to penetration of the electron beam. However, the absence of Si in the Mo rich regions indicates that they are pure Mo which is a bit puzzling. Moreover, the absence of an Al signal is also unexpected. Clearly, further study including the analysis of the sample cross section is necessary to understand the observed changes in coating constitution..

Raman spectroscopy of Si-B pack cementation and then conditioning followed by Al-coating

Raman Spectroscopy is a non-destructive chemical analysis technique which provides detailed information about chemical structure, phase and polymorphy, crystallinity and molecular interactions. It is based upon the interaction of light with the chemical bonds within a material. Raman is a light scattering technique, whereby a molecule scatters incident light from a high intensity laser light source. Most of the scattered light is at the same wavelength (or color) as the laser source and does not provide useful information – this is called Rayleigh Scatter. However, a small amount of light (typically 0.0000001%) is scattered at different wavelengths (or colors), which depend on the chemical structure – this is called Raman Scatter.
A Raman spectrum features a number of peaks, showing the intensity and wavelength position of the Raman scattered light. Each peak corresponds to a specific molecular bond vibration, including individual bonds and groups of bonds such as ring breathing modes, molecular chain vibrations and lattice modes.

Figure 18 shows the Raman spectroscopy of Si-B pack cementation at 1000 °C for 50 h in argon environment on both white and black regions. In both the regions, Si-B pack cementation sample shows borosilica, coesite SiO_2, and MoO_3 phases at the wave numbers of 435 cm^{-1}, 327 and 519 cm^{-1}, and 89 and 119 cm^{-1} respectively [Kon 76, Kin 94, Py 77]. The intensity of phases is much higher in white region rather black region that leads to phase fractions of those phases are very high in white region.

Usually, as per polymorphism of SiO_2 at ambient pressure [Hea 94,Hig 94] (Fig. 19), either tridymite or quartz SiO_2 phase should form after completion of pack cementation process followed by cooling (1000 °C for 50 h followed by 10 °C /min). But, interestingly, the coesite SiO_2 phase is accompanyed by the borosilica phase in Raman spectroscopy which indicates that boria (B_2O_3)/BO_4 network influences the crystal structure of SiO_2 via formation of borosilica phase. An explanation of how the BO_4 network effects the crystal structure of tridymite SiO_2 and formation of coesite can be proposed using the model proposed by Fair [Fai 95] which is shown in Fig. 20.

According to the model proposed by Fair et al. [Fai 95], initially when B is doping into Si at 1000 °C through pack cementation, either boron forms BO_4 network or boron diffuses into tridymite SiO_4 and forms a boron doped SiO_4 network (B-SiO_4). Subsequently, the unpaired electrons of oxygen atoms of the BO_4 networks react with non-bridging oxygens (since the bonding between non-bridging oxygens and Si atoms is very weak as compared to bridging oxygens) of tridymite SiO_4 networks leads to form borosilicate networks (substitutional site) and peroxide defects. Consequently, the destabilized B-SiO_4 networks transform into a coesite SiO_2 ring structure rather quartz during cooling. The transition of BO_4 and tridymite SiO_4 networks into coesite, at substitutional sites and peroxide defect formation are schematically shown in Fig. 21. Afterwards, these peroxide defects are aiding to Mo atoms to diffuse out from Si-B pack cementation and then react with oxygen atoms and form MoO_3 phase that was also appeared in Raman spectroscopy (Fig. 18).

Raman spectroscopy of Si-B pack cementation conditioning at 1300 °C for 2 h in air is shown Fig. 22. In this condition, Raman spectroscopy was done on both shiny and dark regions and those regions were already shown in Fig.2. Si-B pack cementation conditioning sample shows quartz, cristobalite and Al_2O_3 phases at the wave numbers of 128, 206, 354 and 464 cm^{-1}, 230 and 420 cm^{-1}, and 568 and 734 cm^{-1} [Kin 94] along with borosilica, coesite and MoO_3 phases in both the regions.

During Si-B pack cementation conditioning at 1300 °C for 2 h in air, there is a sufficient time for oxygen atoms to diffuse into coesite SiO_2 rings and try to form cristobalite and then, cristobalite network transform into quartz while cooling to room temperature (10 °C /min) as shown in schematic diagram of Fig. 23. The transition of coesite into cristobalite and quartz networks are schematically shown in Fig. 24. Concurrently, Mo from substrate and Al from pack are reacting with oxygen and then try to form MoO_3 and Al_2O_3 phases. The Raman spectra of the coating surface after Si-B pack cementation at 1000 °C for 50 h in an argon environment are shown in figure 18 for the same light (white) and dark (black) regions in Fig.1. In both the regions, the Si-B pack cementation sample shows borosilica, coesite SiO_2, and a trace of the MoO_3 phases at the wave numbers of 449 cm^{-1}, 327 and 519 cm^{-1}, and 89 and 119 cm^{-1}. The appearance of MoO_3 probably originates from redeposition during sample cooling. The intensity of phases is much higher in white region than in the black region. Typically, based upon the polymorphism of SiO_2 at ambient pressure, either tridymite or quartz SiO_2 phases should form after completion of the pack cementation process followed by cooling. Interestingly, Coesite and borosilica phases appeared in the Raman spectra which indicates that boria (B_2O_3) or the BO_4 network may induce changes in the crystal structure of SiO_2. For example, when B is added into Si at 1000 °C, initially it forms a BO_4 network/ B_2O_3 along with SiO_4 /SiO_2. Subsequently, the lone pair electrons of oxygen atoms of the BO_4 networks react with non-bridging oxygens of the SiO_4 networks. Consequently, the SiO_4 networks will be destabilized and form a borosilicate network. On the other hand, the oxygen atoms of the destabilized SiO_4 networks react with the surrounding Si atoms and form a coesite SiO_2 ring structure. The formation of coesite and borosilica network and peroxide defects are schematically shown in Fig.25.

The Raman spectra of the coating following Si-B pack cementation and conditioning at 1300 °C for 2 h in air is shown Fig.26. In this condition, the Raman spectra were taken on both the shiny (light) and dark regions. The sample surface shows quartz, cristobalite and Al_2O_3 along with borosilica, coesite and MoO_3 phases in both the regions. Evidently, conditioning at 1300 °C for 2 h is sufficient time for oxygen atoms in the surrounding air to destabilize the coesite rings through non bridging oxygens to form a cristobalite network (Fig.27)and then while cooling to room temperature, the cristobalite network transforms into quartz as shown in the schematic diagram of Fig.28. Concurrently, Al reacts with oxygen atoms to form Al_2O_3.

Lastly, the Raman spectra of the Al-coating after conditioning and wet oxidation exposure are shown in Fig.29. The sample exhibits the borosilica and coesite phases. The Raman spectra of the Al-Si-B coated samples for 35, 40, 75 h of wet oxidation exposure demonstrated that cristobalite, mullite and MoO_3 phases are present but the borosilica and amorphous SiO_2 (a-

SiO_2) phases were not observed. During wet oxidation, initially OH^- ions react with non-bridging oxygens of coesite ring and form $(OH)_2$ free radicals. These free radicals pull out the Si atoms from ring structure and form Si $(OH)_2$ that then evaporates. This is one of reasons for the weight loss of wet oxidized samples. Subsequently, unstable broken rings transform to stabilize SiO_4 networks and form cristobalite. The cristobalite reacts with Al_2O_3 to form mullite. The Al-coating and conditioning as well as the wet oxidized samples should be repeated for Raman spectroscopy to confirm the phases and the tentative reaction sequences.

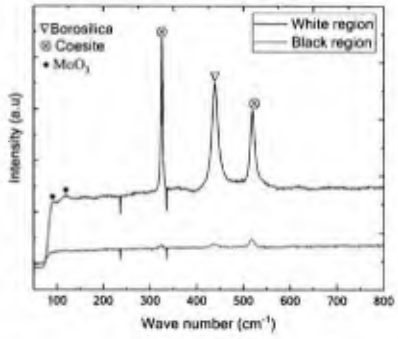

Figure 18 Raman spectra of the Si-B pack cementation coating developed 1000 °C for 50 h in an argon environment

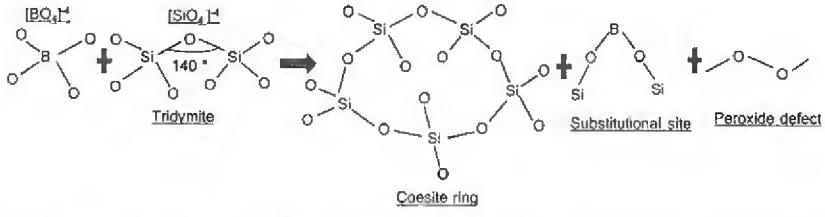

Figure 19 Schematic diagram of coesite ring and borosilica formation during pack cementation

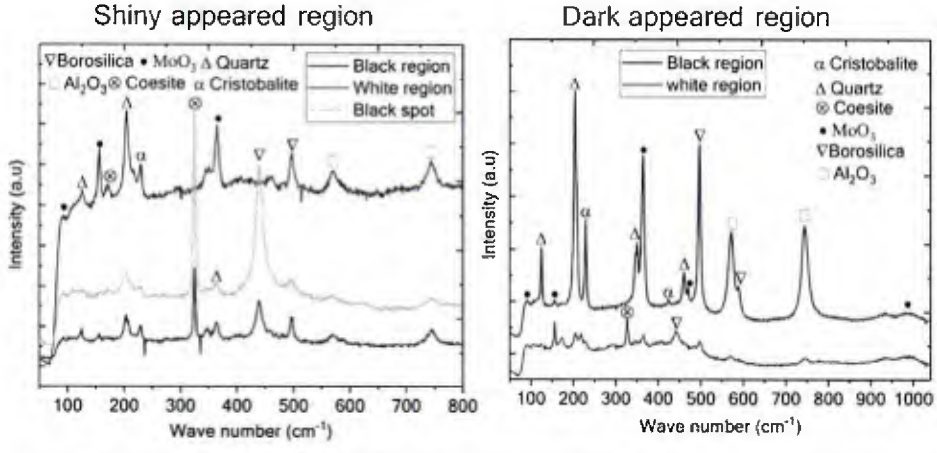

Figure 20 Raman spectra of the Si-B pack cementation coating after conditioning at 1300 °C for 2 h in air

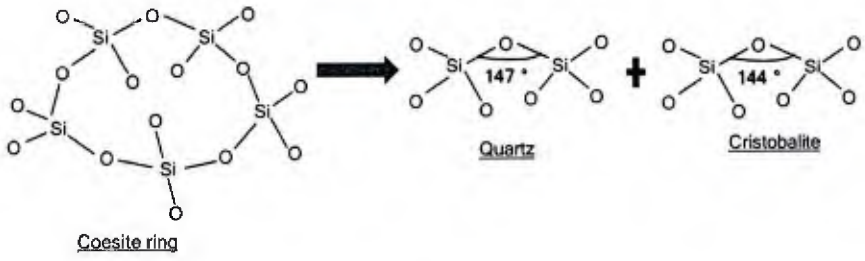

Figure 21 Schematic diagram of quartz and cristobalite formation from coesite ring during pack cementation conditioning

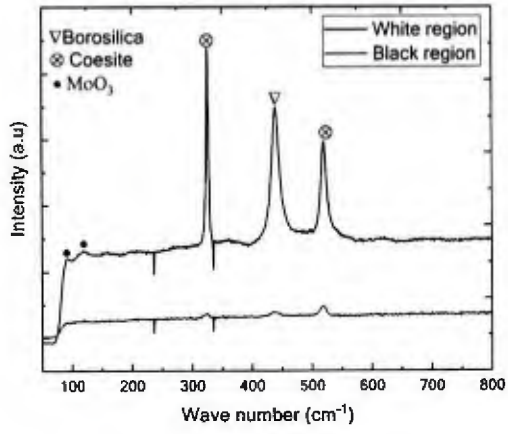

Figure 22 Raman spectroscopy of Si-B pack cementation at 1000 °C for 50 h in argon Environment

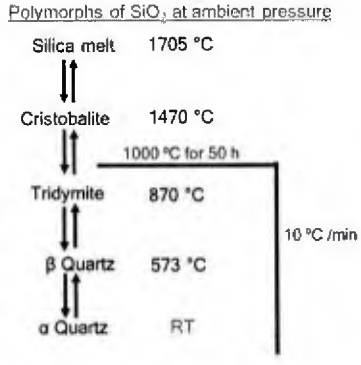

Figure 23 Polymorphs of SiO_2 at ambient pressure showing quartz or tridymite phase forms after pack cementation at 1000 °C for 50 h followed by 10 °C /min.

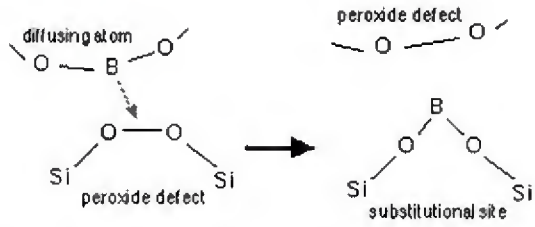

Fig. 24 Boron diffusion in silicon dioxide model proposed by Fair

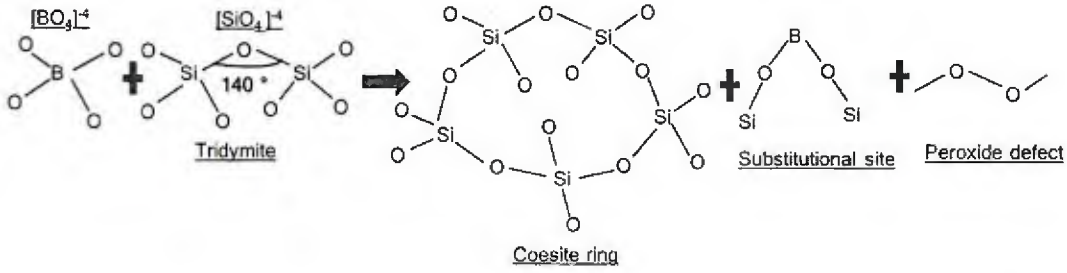

Figure 25 Schematic diagram of coesite ring and borosilica formation during pack cementation

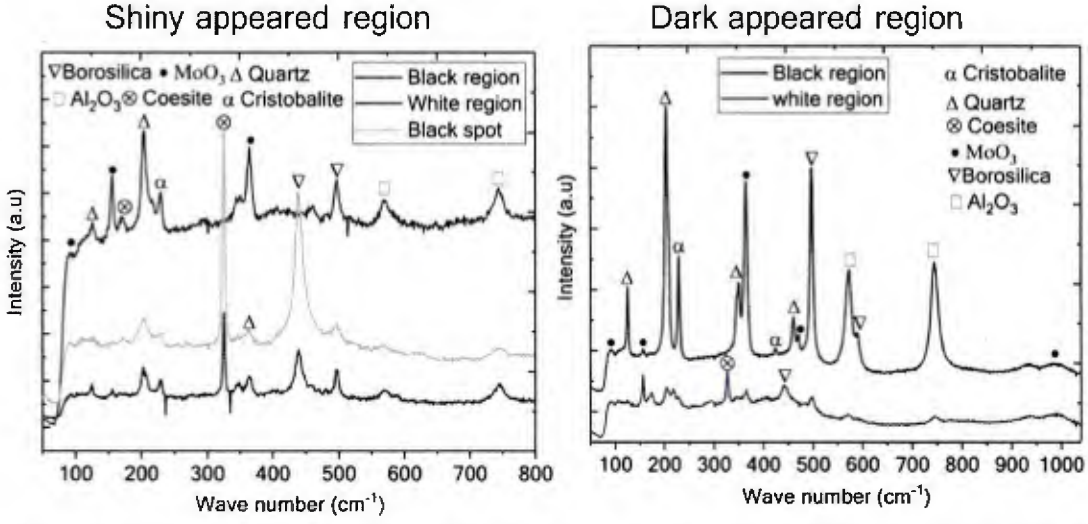

Figure 26 Raman spectroscopy of Si-B pack cementation conditioning at 1300 °C for 2 h in air

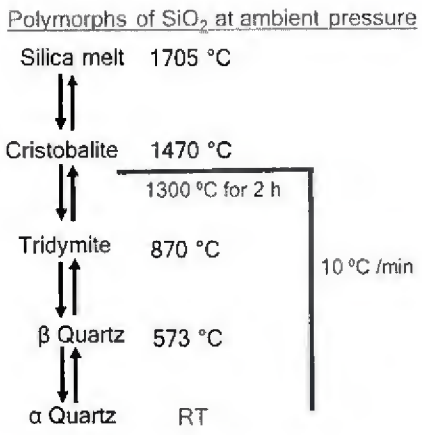

Figure 27 Polymorphs of SiO_2 at ambient pressure showing quartz or cristobalite phase forms after pack cementation conditioning at 1300 °C for 2 h followed by 10 °C /min.

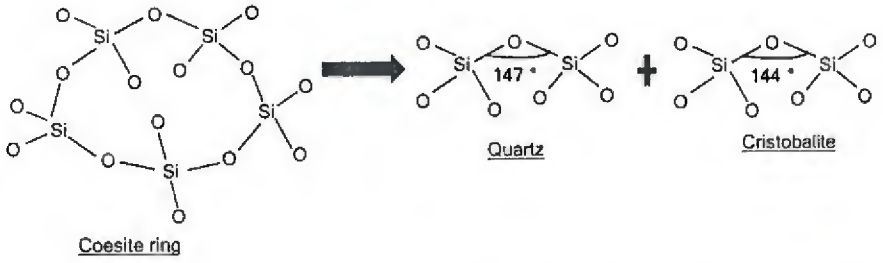

Figure 28 Schematic diagram of quartz and cristobalite formation from coesite ring during pack cementation conditioning

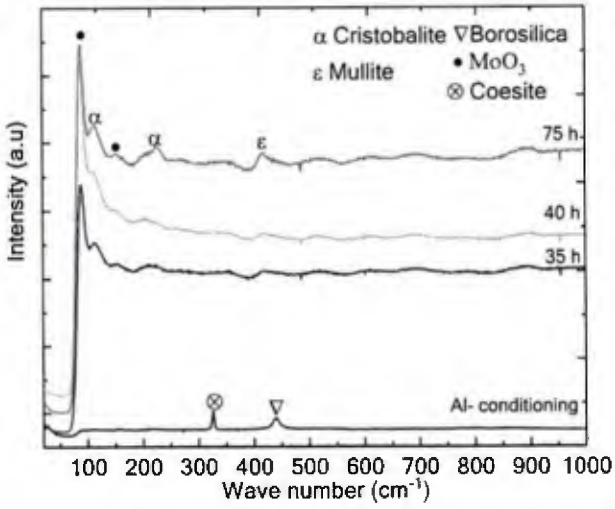

Figure 29 Raman spectroscopy of Al-coating conditioning at 1450 °C for 2 h and wet oxidized samples at 1450 °C for 35, 40 and 75 h in air

Conclusions

The following preliminary conclusions are drawn based on the SEM and Raman spectroscopy analysis on Si-B pack cementation followed by Al coatings and wet oxidation on Mo substrate.

- $MoSi_2$ and Coesite phases are formed during Si-B pack cementation.
- After Si-B pack cementation conditioning, coesite, cristobalite, quartz and borosilicate phases were observed.
- The quartz phase formed during Al-coating.
- Coesite, mullite and borosilica phases are formed after Al-coating conditioning.
- During wet oxidation, OH^- ions attack the non-bridging oxygens of coesite and form $Si(OH)_2$ and the ring structure transforms into cristobalite.

While this initial study has yielded new insight on the evolution of the coating structure during synthesis, conditioning and oxidation exposure further study is necessary to elucidate the details of the structural transitions.

3.3 Adapted Mo-Si-B + Al Coating for Protection of SiC-Based Materials in Active Oxidation Environments

SiC-based materials are being considered for several aerospace applications including exposure to very high temperatures (>1500°C) and low partial pressures of oxygen. In these environments, SiC is prone to a degrative oxidation mechanism known as active oxidation. At higher oxygen potentials, it is well established that SiC oxidizes to form the condensed phase $SiO_2(s)$ in reaction (1) [Jac 11]:

$$SiC\ (s) + 3/2O_2\ (g) \rightarrow SiO_2\ (s) + CO\ (g) \qquad (1)$$

This is termed "passive oxidation." However, at lower oxygen potential and high temperatures, SiC may oxidize to form volatile SiO(g) as in reaction (2) [Jac 11]:

$$SiC\ (s) + O_2\ (g) \rightarrow SiO\ (g) + CO\ (g) \qquad (2)$$

This is termed "active oxidation" and leads directly to the erosion of the SiC substrate.

It is well known that there is a "hysteresis" between the active-to-passive transition and the passive-to-active transition. In a study by Myers and Jacobson [Jac 11] and a two-part study by Jacobson, Harder and Myers [Jac 13,Har 13], it was concluded that the active-to-passive and passive-to-active transition point is governed by the same interfacial reaction at the SiC/SiO2 interface, but occur at different oxygen potentials. This interfacial reaction is shown in reaction (3):

$$SiC\ (s) + 2SiO_2\ (s) \rightarrow 3SiO\ (g) + CO\ (g) \qquad (3)$$

At high oxygen potentials, SiO(g) is unstable and is immediately oxidized to SiO2, suppressing the interfacial reaction. As the oxygen potential is lowered, the interfacial reaction will proceed through the cracks in the SiO2 scale [Har 13]. The pressure build-up of SiO(g) and CO(g) at the SiC/SiO2 interface, as well as the thinning of the SiO2 scale due to reaction with SiC, will eventually cause the SiO2 scale to rupture [Har 13]. The exposed SiC substrate will then oxidize according to reaction (2).

The passive-to-active transition is of more concern than the active-to-passive transition when looking at SiC to be used for hypersonic flight. During application, the substrate would experience low temperatures and high oxygen potentials (passive conditions) initially but would gradually reach high temperatures and low oxygen potentials (active conditions) during the duration of the flight, undergoing the passive-to-active transition. Traditionally, the analysis of the active/passive transition of SiC comes from Wagner's Theory regarding the active/passive transition in Si [Wag 58]. It is widely accepted that the passive-to-active transition should be similar for Si, SiC and Si_3N_4 [Heu 90]. However, more recent studies show a high degree of discrepancy, suggesting that the theory is not all encompassing.

A study by Jacobson [Jac 11] compiles the work of many, trying to discern the active/passive transition. Figure 30 show a very wide range of results when looking at temperature and oxygen potential alone. This suggests more information is needed and that other parameters should be considered. Some of the potentially most influential parameters include the effect of total pressure and the effect of impurities in passive silica.

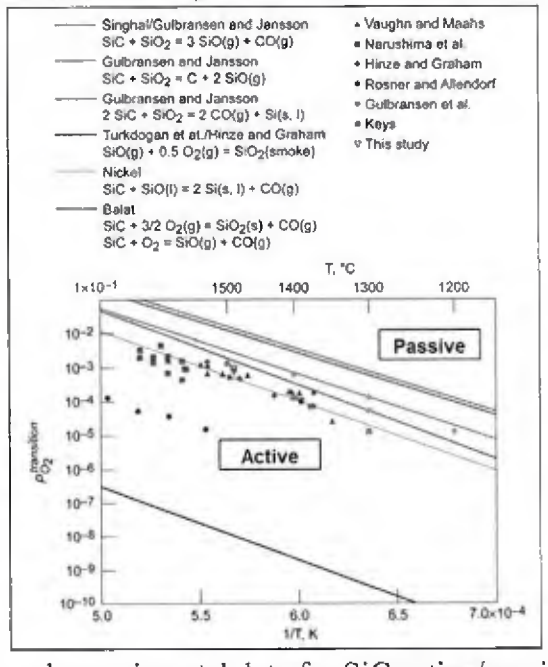

Figure 30. Theoretical and experimental data for SiC active/passive transitions [Jac 11].

Total pressure is an important parameter to consider, as it plays a major role in the disruption of the passive $SiO_2(s)$ outer layer in the passive-to-active transition. The proposed mechanism for the passive-to-active transition is shown in Figure 31 [Har 13]. CO(g) and SiO(g) form at the interface of SiC and $SiO_2(s)$. Some of the gas will escape through the cracks, leading to SiO_2 rod formation once SiO(g) reaches higher oxygen potentials. However, the developing pressure can become great enough to ablate the passive layer, and the pressure at which this occurs is depend on the total surrounding pressure. While some studies have used reduced total pressures to achieve low oxygen potentials, most use gas mixtures at atmospheric pressures.

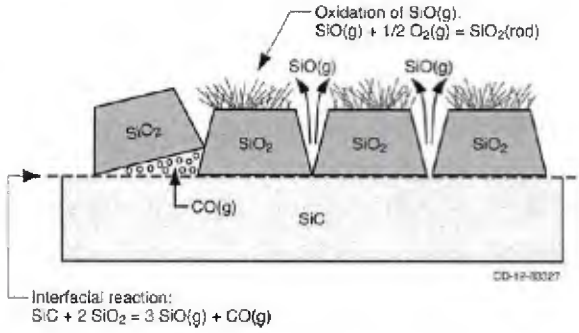

Figure 31. Probable mechanism for the passive-to-active transition of SiC [Har 13].

Even minor amounts of impurities in the passive $SiO_2(s)$ can have a large effect on the diffusivity of oxygen and therefor on the passive-to-active transition in SiC. Being that the passive layer is amorphous, there are two main mechanisms of oxygen diffusion [Lam 93]: Mobility through the open space channels in the low-density areas of glass network or oxygen self-diffusion through the bonded oxygen in the glass network. Impurities can cause significant change in these diffusion mechanisms by either modifying the glass network or disrupting oxygen mobility through the channels. Dopants such as B, Ge, and As are describes as network formers, since they will form oxides that contribute to the glass structure. Network modifiers, such as Na, K, and Mg form oxides that disrupt the glass structure. Replacing a Si atom with one of these will cause an increase in the number of non-bridging oxides, or oxides that connect one SiO_4 tetrahedra with another. Monovalent ions will form one non-bridging oxygen per cation, and divalent ions will form two non-bridging oxygens. This leaves larger channels in the network, increasing oxygen mobility. Elements such as Al, Ti, and Zr form what is known as intermediate oxides. These oxides would normally not be glass forming however can enter the network by replacing a Si atom. When this occurs, an additional cation will have to occupy nearby channel spaces in order to maintain charge neutrality. This in turn blocks oxygen mobility in the channels, as well as increases the activation energy to replace an oxygen in the glass network due to attraction between the cation and bonded oxygen [Lam 92,Wan 06].

Mo-Si-B based alloy multilayer coatings have been proven to be robust in oxidative environments at extreme temperatures. They show promise as a solution to preventing active oxidation of SiC, as they show good compatibility. This coating is applied to SiC by a multi-step process. Mo is first deposited on SiC, which can be done via slurry sintering, yielding a continuous layer of well bonded Mo on SiC over 100 μm thick. Next, Si and B are incorporated into the Mo coating by pack cementation in an alumina filler. During the application, an outer layer of $MoSi_2$ develops followed by a Mo-rich silicide layer of Mo_5Si_3 (T1) phase with dispersoids of the MoB phase. Finally, during a conditioning treatment that involves exposure to air at high temperature, the coating structure evolves into layers: an outer layer of borosilica glass which provides self-healing capabilities, an underlying layer of B-saturated Mo_5Si_3 (T1) which functions as the oxidation resistant layer and the borosilicide Mo_5SiB_2 (T2) phase which

forms in situ in contact with the substrate and serves as a diffusion barrier for both silicon and boron [Sak 08,Nun 00].

Thermogravimetric analysis was conducted on oxidized CVD SiC, Mo-Si-B coated CVD SiC and Mo-Si-B + 5 wt% Al coated CVD SiC at 1400°C in flowing 100 ppm O_2/balance Ar gas. The results are plotted in Figure 32. It is clear that the Mo-Si-B + 5 wt% Al sample has superior resistance to mass loss in active oxidation conditions, in terms of steady state mass loss (~$9x10^{-6}$ mg/mm^2-min) as well as total mass change. Post-test plan view SEM micrographs showed large grains of alumina and regions of aluminoborosilica glass. The cross-sectional view in Figure 33 shows a layer of alumina on the surface of the sample, with intermixed $MoSi_2$ and Mo_5Si_3 and aluminoborosilica underneath. The aluminum content in the aluminoborosilica layer was ~5-10 at%, as determined by EDS. While this preliminary result is encouraging and appears to support our working hypothesis, a more complete systematic study is necessary to define and confirm the beneficial effect of Al and other additions to the MoSiB based coating performance.

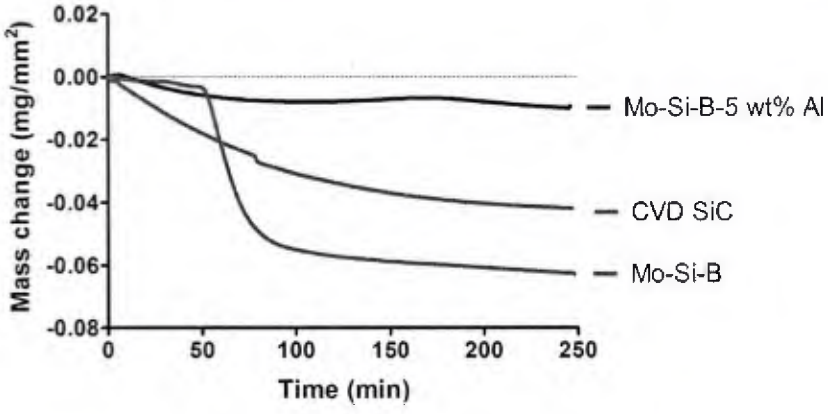

Figure 32. In situ mass change results from exposure of oxidized CVD SiC ("CVD SiC"), Mo-Si-B coated CVD SiC ("Mo-Si-B") and Mo-Si-B + 5 wt% Al coated CVD SiC ("Mo-Si-B-5 wt% Al") to 100 ppm O_2/balance Ar flowing at 100 mL/min at 1400°C for 4 hours each.

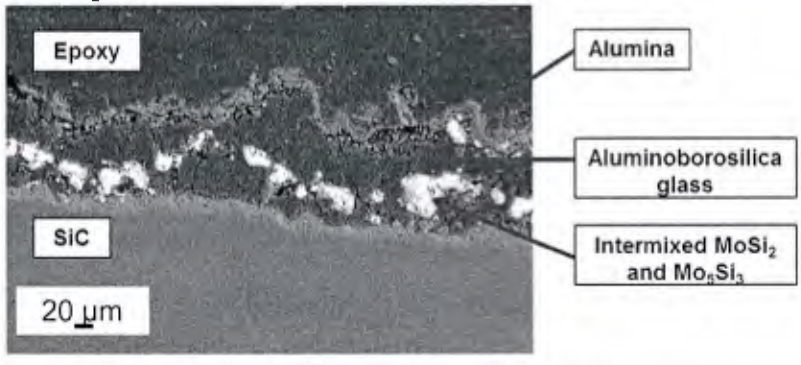

Figure 33. Cross-sectional backscattered SEM image of Mo-Si-B + 5 wt% Al coated CVD SiC after exposure to 100 ppm O_2/balance Ar flowing at 100 mL/min at 1400°C

3.4 Creep of an Oxidation Resistant Coated Mo-9Si-8B Alloy

Numerous studies on high temperature oxidation behavior in Mo-Si-B alloys reveal that the alloy compositions with the best performance do not have satisfactory mechanical properties (notably low temperature ductility and fracture toughness) due to the high volume fraction of silicide phases needed for the oxidation resistance [4]. Similarly, alloy compositions with satisfactory mechanical properties usually exhibit poor oxidation resistance due to the continuous Mo_{ss} phase [5]. One strategy to address this dilemma is to apply an oxidation resistant coating. A successful coating has been developed based upon a co-deposition of B and Si by pack cementation that exhibits thermodynamic and mechanical compatibility and self-healing [6]. The coating has been demonstrated to provide a robust environmental resistance to attack by oxidation, CMAS, hot corrosion by molten salt and water vapor [3]. Besides the environmental resistance it is important to assess the influence of the coating on the mechanical behavior. In this work it is demonstrated that the high temperature creep performance of a Mo-9Si-8B alloy is essentially unaffected by the coating, proofing the protective capability of the coating under application relevant conditions with superimposed plastic deformation.

Experimental Procedures

The Mo-9Si-8B alloy (in at.%) was manufactured from elemental powders Mo, Si and B with purities of 99.95%, 99.9% and 98% respectively. Mechanical alloying was carried out using a planetary ball mill (Retsch PM 400) with WC balls, a powder to ball ratio of 1:12 and a speed of 200 rpm [5]. Compaction was carried out using the field assisted sintering technique (FAST) at 1600 °C and 50 MPa for hold times of 15 min. As a result, buttons with a diameter of 50 mm and a height of 10 mm and a residual porosity of < 2 % were produced [7].

After homogenization treatment at 1600 °C for 100 h, dogbone shaped tensile samples with a total length of 35 mm, a gage length of 15 mm and a square cross-section of 3 x 4 mm^2 were manufactured from above buttons by EDM (see insert in fig. 3). Prior to pack cementation the gage section of these samples was ground to a 2500 grit finish. The tensile samples were then embedded in a powder mixture consisting of 62.5 wt.% Al_2O_3, 35 wt.% Si and B mixture (Si/B = 35/1) and 2.5 wt.% NaF for pack cementation in an Ar atmosphere at 1000 °C for 40 h to co-deposit the Si and B. A detailed description of the pack cementation process can be found elsewhere [8,9].

Tensile creep tests were on the one hand carried out under constant true stresses at 1200 °C in a Zwick universal testing device equipped with a Maytec vacuum furnace (<10^{-4} Pa), in order to use the continuously monitored creep strain by inductive displacement transducers attached to the gage section as a proof that the coating does not affect the creep behavior. For further details see [10]. On the other hand, further creep tests were performed in air in order to amplify the adhesion and self-healing capability of the coating.

Results

The initial coating structure after pack cementation is displayed in fig. 34a) where (from left to right) an outer amorphous borosilica layer is in contact with a $MoSi_2$ layer which in turn is in contact with a mixed MoB and Mo_5SiB_2 (T_2) layer before reaching the three phase Mo_{ss} + Mo_3Si

+ T_2 substrate. After conditioning at 1400 °C for 10 h in air the coating structure evolves into the structure shown in fig.34b) where the top and bottom portion of the $MoSi_2$ layer converts to Mo_5Si_3 which is followed by a MoB/T_2 layer before reaching the substrate. Exposure of samples with this coating at 1300 °C for extended periods of 500 hours (without mechanical loading) indicated a small mass change of less than 0.3 mg/cm^2 [8x].

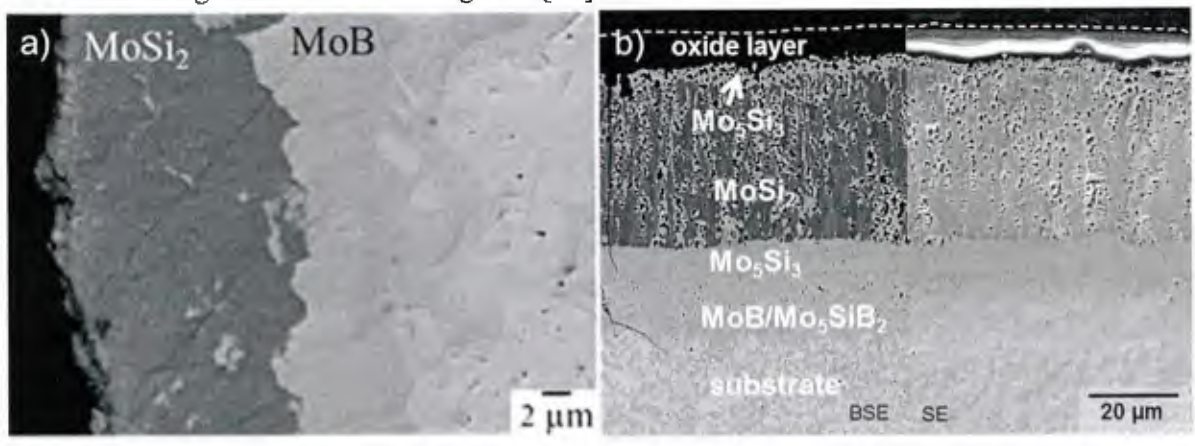

Fig. 34 a) BSE-micrograph of the as-packed sample [3], b) BSE-micrograph left and SE-micrograph right of the conditioned coated Mo–9Si–8B sample

Following exposure at 1200 °C in air and under an applied stress of 50 MPa the sample exhibited a full retention of the coating after 6 % plastic strain as shown in plan view in fig. 35a) and in cross section in fig. 35b). There was no evidence for coating spallation or oxidation of the substrate. Some crack development was detected normal to the tensile direction (fig.35b) but it is evident that the borosilica was able to form and flow into the cracks as a self-healing process (errors in fig. 35b II). In essence the same observations were made for creep tested samples at 1200 °C under a stress of 100 MPa.

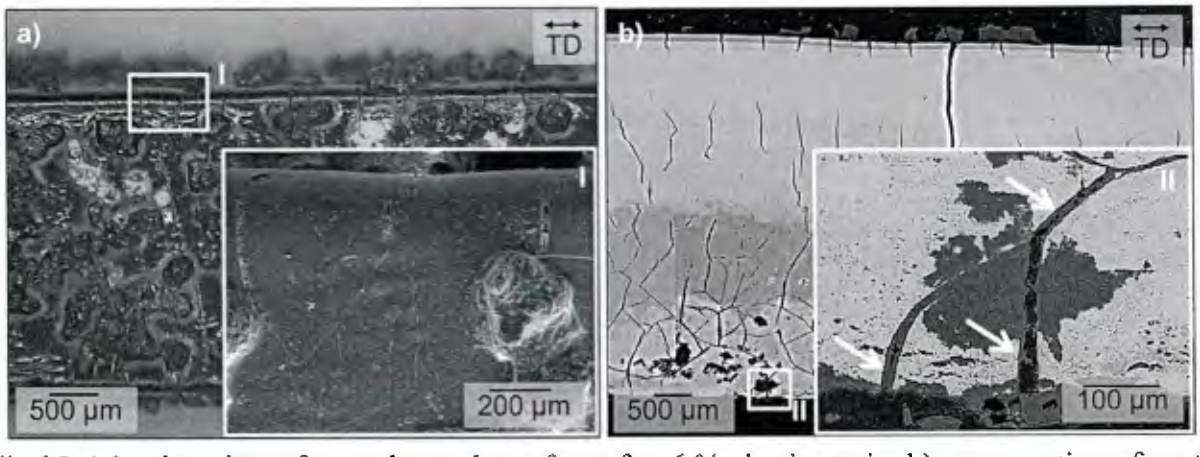

Fig.35 a) In plan view of coated sample surface after 6 % plastic strain, b) cross section of coated sample after 6 % plastic strain illustrating the flow of borosilica to fill cracks (TD refers to tensile direction)

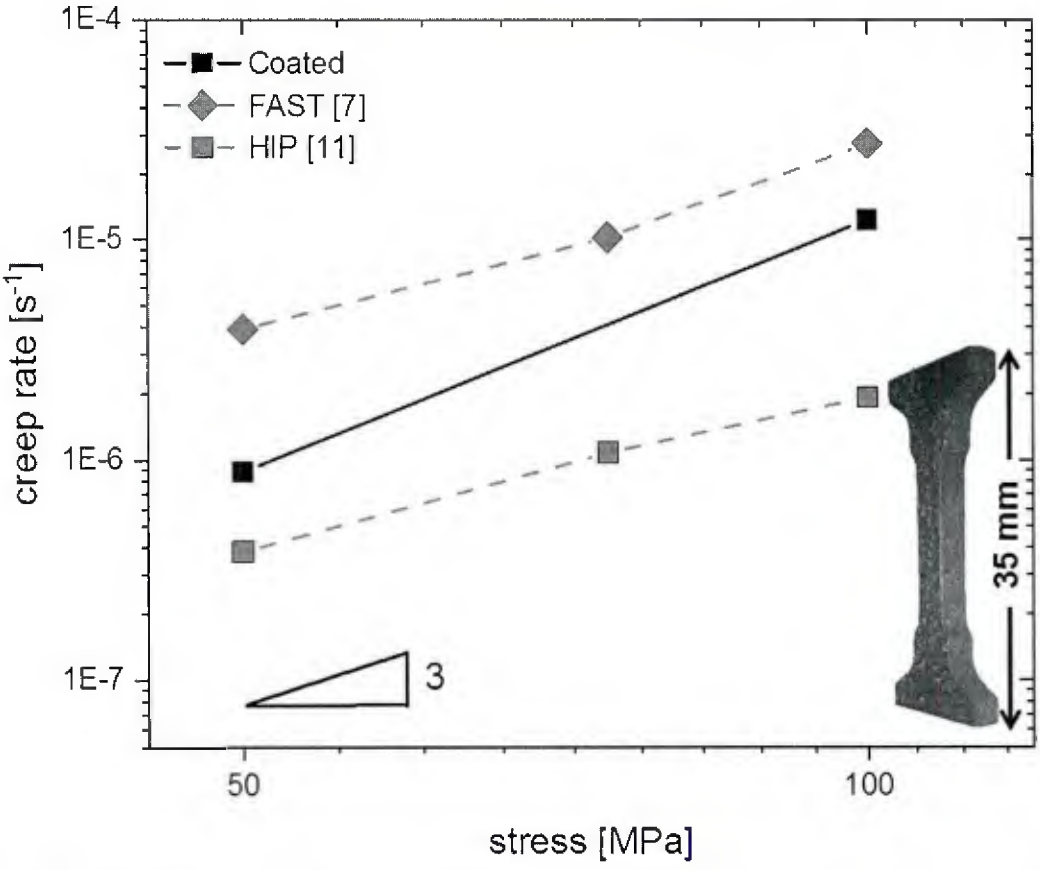

Fig. 36) Double logarithmic plot of the minimum strain rate vs. applied stress at 1200 °C for Mo-9Si-8B alloys with different grain sizes. The grain size for the uncoated FAST sample is 0.75 µm [7] and that for the uncoated HIP sample is 1.5 µm [11] while that for the coated sample has an intermediate value of about 1.3 µm.

The minimum creep rates for the coated samples were compiled with literature results obtained on uncoated material plotted in fig. 36) versus the applied creep stress. Two conclusions can be drawn from this comparison: (i) as discussed in [7] for a series of Mo-9Si-8B alloys with different Zr additions, a clear tendency for increased creep rates with decreasing grain size is noted. This was explained in [7] by the increased contribution of grain boundary sliding processes and our coated samples fit very well into this trend; (ii) no obvious impact of the additional coating on the course of the minimum creep rates is found which expresses itself in the very similar stress exponents ranging between 2.3 and 3.7. This supports the above observations in that the coating is well adherent and obviously able to protect the underlying substrate well.

Conclusions

The effect of an oxidation resistant Mo-Si-B based coating on the deformation of a Mo-9Si-8B alloy was evaluated during tensile creep experiments at 1200 °C. The observed creep rates for coated samples at stresses between 50 and 100 MPa are consistent with the reported values for uncoated samples demonstrating that the coating had a negligible effect on the creep behavior. At a plastic strain of 6 % some cracking was observed normal to the tensile direction, but the cracks

were filled by flowing borosilica glass indicating a self-healing capability. The coating structure was maintained during creep deformation.

References

[1] J. H. Perepezko, The Hotter The Engine, The Better: Science 326 (2009), 5956-5957.

[2] A.P. Alur, N. Chollacoop, K.S. Kumar: High-temperature compression behavior of Mo-Si-B alloys, Acta Materialia,52(19) (2004), 5571–5587.

[3] J. H. Perepezko, R. Sakidja: Extended Functionality of Environmentally-Resistant Mo-Si-B-Based Coatings, JOM, 65 (2013) 307-317.

[4] J.H. Schneibel, R.O. Ritchie, J.J. Kruzic, P.F. Tortorelli: Optimization of Mo-Si-B intermetallic alloys, Metall. Mater. Trans. A36 (2005), 525-531.

[5] M. Krüger, S. Franz, H. Saage, M. Heilmaier, J.H. Schneibel, P. Jéhanno, M. Böning, H. Kestler: Mechanically alloyed Mo-Si-B alloys with a continuous α-Mo matrix and improved mechanical properties, Intermetallics 16 (2008), 933-941.

[6] J.H. Perepezko: Surface Engineering of Mo-Base Alloys for Elevated-Temperature Environmental Resistance, Ann. Rev. Mater. Res., 45 (2015) 519-542.

[7] C. Hochmuth, D. Schliephake, R. Völkl, M. Heilmaier, U. Glatzel: Influence of zirconium content on microstructure and creep properties of Mo-9Si-8B alloys, Intermetallics 48 (2014), 3-9.

[8] A. Lange, M. Heilmaier, T.A. Sossaman, J.H. Perepezko, Oxidation behavior of pack-cemented Si-B oxidation protection coatings for Mo-Si-B alloys at 1300°C, Surf. Coat. Tech. 266 (2015), 57-63.

[9] D. Schliephake, C. Gombola, A. Kauffmann, M. Heilmaier, J.-H. Perepezko, Enhanced Oxidation resistance of Mo-Si-B-Ti Alloys by Pack Cementation, Oxid. Met. 88 (2017), 267-277.

[10] D. Schliephake, M. A. Azim, K. v. Klinski-Wetzel, B. Gorr, H.-J. Christ, H. Bei, E. P. George, M. Heilmaier: High-Temperature Creep and Oxidation Behavior of Mo-Si-B Alloys with High Ti Contents, Metall. Mater. Trans. 45A (2014), 1102-1111.

[11] M. Krüger, D. Schliephake, P Jain, K,S, Kumar, G, Schumacher, M, Heilmaier, Effects of Zr Additions on the Microstructure and the Mechanical Behavior of PM Mo-Si-B Alloys, JOM 65 (2013), 301-306.

3.5 Coating of Vanadium and Chromium Alloys

Recently, creating a more effective means of Mo addition onto the substrate of other materials has been restrictive. Alloys that contain Mo or do not have much of a mismatch in their atom arrangement and size have shown considerable progress for using a Mo pack. A recent vanadium alloy was successfully coating with Mo using a Mo pack and finishing up with a Si-B pack. Successfully conditioning these samples has been difficult.

Multiple vanadium samples with Mo packs instead of slurry coats were produced with only one sample passing conditioning. With the many failures that Mo packs have presented it is likely that a different avenue of addition onto the coating is necessary. A new approach based upon the use of a Mo slurry with Hydroxypropyl Cellulose(HCP) has shown results that far exceed previous surface coating attempts by other means as shown in fig. 37.

Figure 37: SEM image of Mo slurry coating using HPC on a V substrate.

As figure 37 shows, a single coating that is about 30 microns thick and can be varied by changing the temperature and time of the heating cycle. This process takes 4 hours for completion. Furthermore, this process has been successfully implemented on a number of substrates. Figure 38 shows successful adhesion onto a Cr 9 a/o Si alloy.

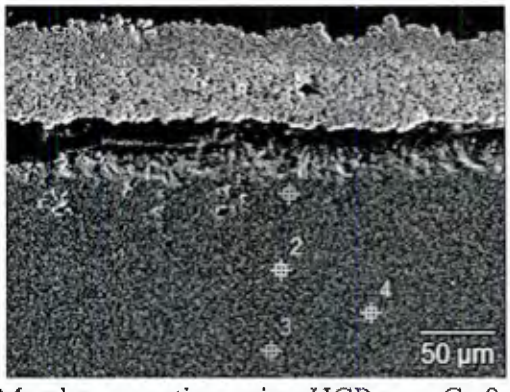

Figure 38: SEM imaging of Mo slurry coating using HCP on a Cr-9 a/oSi alloy.

Using this new method will allow for a fine tuning the amount of Mo that is deposited. Currently multiple slurry coatings using HCP and 35:1 pack cementation have been completed and are awaiting analysis. With this new Mo application, it is likely that a host of many new substrates that previously failed may now be accomplished successfully.

4.Publications and Presentations for the Current Program

4.1Publications

1. "Hot Corrosion of Mo–Si–B Coatings", M. Taylor and J.H. Perepezko, Oxidation of Metals, 87, 705–715 (2017).

2. "Enhanced Oxidation Resistance of Mo–Si–B–Ti Alloys by Pack Cementation", D. Schliephake, C. Gombola, A. Kauffmann, M. Heilmaier and J. H. Perepezko, Oxidation of Metals, 88, 267–277 (2017).
3. "Environmental Resistant Coatings for High Temperature Mo and Nb Silicide Alloys", J.H. Perepezko, MRS Advances, 2: 25, 1323-1334 (2017).
4. Environmentally Resistant Mo-Si-B-Based Coatings, J.H. Perepezko, T.A. Sossaman, M. Taylor, Journal of Thermal Spray Technology, 26, 5, 929-940 (2017).
5. Deformation behavior of Mo_5SiB_2 N.I.Medvedeva, O.Y.Kontsevoi, A.J.Freeman and J.H.Perepezko, Intermetallics, 90, 54-57 (2017).
6. High temperature environmental resistant Mo-Si-B based coatings, J.H. Perepezko, Int.Jnl. Refractory Metals and Hard Mater., 71 246-254 (2018) DOI: 10.1016/j.ijrmhm.2017.11.033
7. Oxidation resistance of a Mo-W-Si-B alloy at 1000–1300° C: The effect of a multicomponent Mo-Si-B coating,G Ouyang, PK Ray, S Thimmaiah, MJ Kramer, M Akinc, P Ritt, JH Perepezko, Applied Surface Science 470, 289-295 (2019)
8. Creep of an oxidation resistant coated Mo-9Si-8B alloy, C Gombola, D Schliephake, M Heilmaier, JH Perepezko, Intermetallics 120, 106743(2020)
9. Resistance of a Mo–Si–B-Based Coating to Environmental Salt-Based Hot Corrosion, E Auchter, M Taylor, JH Perepezko, Oxidation of Metals, 1-13(2020)
10. G. Hasemann, C. Harris, M. Krüger, J. H. Perepezko, "Coating Reactions on Vanadium and V-Si-B Alloys during Powder Pack-Cementation", Materials, *13*(18), 4099 (2020)

4.2 Patents

US Patent 10,385,437, Synthesis of metal-oxygen based materials with controlled porosity by oxidative dealloying, JH Perepezko

3.3 Presentations

1. Environmental Resistant Mo-Si-B Based Coatings, J.H. Perepezko, T.A. Sossaman , M. Taylor, 19th Plansee Seminar, Reutte, Austria, May 2017.
2. The Effect of Pack-Cementation Coatings on the Oxidation Resistance of Mo-Si-B Based Alloys, J. H. Perepezko, D. Schliephake, C. Gombola, M. Heilmaier, TMS 2017 Annual Meeting, Symposium: Materials for High Temperature Applications: Next Generation Superalloys and Beyond San Diego, CA, February 27-March 2, 2017
3. "Phase Stability in Refractory Metal Silicides" J.H.Perepezko, MS&T, Portland,OR October 2019
4. "High Temperature Mo-Si-B Alloys – Phase Stability and Environmental Resistance" ASM International Cleveland Chapter, Zay Jeffries Night April 22,2019
5. "Environmental Resistance and Microstructure Design in Mo-Si-B Alloys", L.Liu, J.H. Perepezko, MS&T conference- I gave virtual presentations, November 2020

5. References

[Abd 07] M. Abdel-Baki, F.A. Abdel-Wahab, A. Radi, F. El-Diasty, J. Phys. Chem. Solids 68, (2007) 1457.

[Aki 99] Akinc, M., et al., Mat. Sci. Eng. A 261 16-23 (1999).

[Aki 08] M. Akinc, Z.H. Tang, A.J. Thom, M.J. Kramer, Intermetallics 16, 1125-33 (2008)

[Ash 69] R. L. Ashbrook, "A survey of salt deposits in compressors of flight gas turbine engines," p. NASA TN D-4999, Jan. 1969.

[Ayg 07] A. Aygun, A.L. Vasiliev, N. P. Padture and X. Ma, Acta Mater. 55, 6734 (2007).

[Bac 86] Backhaus-Ricoult, M. and B. Bunsenges (1986). Phys. Chem. 90: 684.

[Ban 86] N.P. Bansal, R.H. Doremus, Handbook of Glass Properties, Academic Press, Florida, 1986.

[Bar 40] Barrett, H.M., Birnie, A.W., Cohen, M., J. Amer. Chem. Soc., 62, p.2839-44 (1940).

[Bat 06] C. Batista, A. Portinha, R.M. Ribeiro, V. Teixeira and C.R. Oliveira, Surf. Coat Technol., 200, 6783 (2006).

[Ber 97] D. M. Berczik, US Patent 5,595,616 (1997), and 5,693,156 (1997).

[Bir 83] Birks, N. and G. H. Meier (1983). Introduction to High Temperature Oxidation of Metals. London, UK, E. Arnolds Ltd.: 54.

[Bla 01] P. Blaha, K. Schwarz, G.K.H. Madsen, D. Kvasnicka and J. Luitz *WIEN2k, An Augmented Plane Wave Plus Local Orbitals Program for Calculating Crystal Properties*, Vienna University of Technology, Austria (2001).

[Bor 96] Borom, M.P., C.A. Johnson and L.A. Peluso, (2006) Surf. Coat Technol., 86-86: 6783.

[Bor 93] Norman Bornstein, Hilton Roth, and Roscoe Pike, "Vanadium Corrosion Studies," ONR Contract N00014-89-C-0053, United Technologies Research Center, East Hartford, CT, Jun. 1993.

[Bor 97] Bornstein, N.S. and Allen W.P., Mat. Sci. Forum, 251-254,127(1997)

[Boe 92] Boettinger, W. J., J. H. Perepezko, et al. (1992). Mater. Sci. and Eng. A155: 33.

[Bru 92] Brumm, M. W. and H. J. Grabke (1992). Corrosion Science 33(11): 1677.

[Cha 09] L. Charpentier, A. Maitre, M. Balat-Pichelin, S. Foucaud, F. Audubert, Scripta Mater. 60, 481-484 (2009).

[Che 00a] Y.S. Cheong, P. Mukundhan, H.H. Du, S.P. Withrow, J. Am. Ceram. Soc. 83, 154-60 (2000).

[Che 00b] Y.S. Cheong, P. Mukundhan, H.H. Du, S.P. Withrow, J. Am. Ceram. Soc. 83, 161-5 (2000).

[Che 06] Chen, X., Surf. Coat. Tech., 2006. **200**(11): p. 3418-3427.

[Che 09] Z. Chen, S. Speakman, J. Howe, H. Wang, W. Porter and R. Trics, J. European Ceram. Soc., 29, 1403-1411 (2009).

[Che 11] X. Chen, Y. Zhao, L. Gu, B. Zou, Y. Wang and X. Cao, Corrosion Sci., 53, 2335-2343 (2011).

[Cho 93] Chou, T. C. and T. G. Nieh (1993). "Pesting of the high-temperature intermetallic MoSi2." Journal of Metals 45(12): 15-20.

[Bal 10] C. W. Bale *et al. FactSage*. (2010).

[Bur 10] S. Burk, B. Gorr, H.J. Christ, Acta Mater. 58, 6154-65 (2010)

[Coc 95] Cockram, B. V. and R. A. Rapp (1995). Metall. Mater. Trans. A 26A: 777.

[Dea 79] John A. Dean, "Standard Thermodynamic Values," in *Lange's Handbook of Chemistry*, 11th ed., New York, New York: McGraw-Hill, 1979, pp. 9:4-9:128.

[Dim 92] Dimiduk, D. M., D. B. Miracle, et al. (1992). Mater. Sci. and Tech. 8: 367.

[Dow 14] Downs, I. P., Perepezko, J. H., Sakidja, R. & Choi, S. R. Suppressing CMAS attack with a MoSiB-based coating. *Surf. Coat. Technol.* **239,** 138–146 (2014).

[Dre 10] Drexler, J.M., et al., Acta Mater., 2010. **58**(20): p. 6835-6844.
[Dys 90] Dyson, B. F. and M. M. Lean (1990). JISI Int. 30: 802.
[Eat 02] H. E. Eaton and G. D. Linsey, J. European Ceramic Society, v.22 [14-14], p.274102747 (2002)
[Ebe 91] Ebert H and Zeller R, http://olymp.cup.uni-muenchen.de/ak/ebert/SPR-TB-KKR/ (1991)
[Eli 02] Eliaz, N., Shemesh, G. & Latanision, R. M. Hot corrosion in gas turbine components. *Eng. Fail. Anal.* **9,** 31–43 (2002).
[Eva 01] A.G. Evans, D.R. Mumms, J.W. Hutchinson, G.H. Meier and F.S. Pettit, Prog. Mater. Sci. 46, 505 (2001).
[Eva 07] Evans, A.G. and J.W. Hutchinson, Surf. Coat. Tech., 2007. **201**(18): p. 7905-7916.
[Fai 95] R. Fair, Unified model of boron diffusion in thin gate oxides: effects of f, h_2, n, oxide thickness and injected Si interstitials", Technical Digest, International Electron Devices Meeting, (1995) 85.
[Fen 09] T. Feng, H.J. Li, Q.G. Fu, X.H. Shi, K.Z. Li, Surf. Rev. Lett. 16, 223-9 (2009)
[Fri 98] H. Fritze, J. Jojic, T. Witke, C. Ruscher, S. Weber, S. Scherrer, R. Weiss, B. Schultrich, G. Borchardt, J. Eur. Ceram. Soc. 18, 2351-64 (1998)
[Fu 10] Q.C. Fu, H.J. Li, Y.J. Wang, K.Z. Li, J. Tao, Surf. Coat. Tech. 204, 1831-5 (2010).
[Gol 83] D. S. Goldman, J. Am Ceram. Soc., 66 (1983), pp. 205-9.
[Gon 92] J. *González* et al., Phys. Rev. Lett. 69, 172 (*1992*)
[Gul 79] Gul (1979). Mechanisms of Oxidation and Hot Corrosion of Metals and Alloys at Temperatures of 1150 and 1450K under Flow. Materials Research Symposium, National Brueau of Standards.
[Gul 64] E.A. Gulbransen, K.F. Andrew, F.A. Brassart, J Electrochem Soc, 111 (1964) 103-109.
[Hab 12] M.H. Habibi, L. Wang and S.M. Guo, J. European Ceram Soc., 32, 1635-1642 (2012).
[Har 11] Harder, B.J., et al., J. Amer. Cer. Soc., 2011. **94**: p. S178-S185.
[Har 13] B. Harder, N. Jacobson, D. Myers. Oxidation Transitions for SiC Part II. Passive-to-Active Transitions. J Am Ceram Soc 2013, 96(2):606-612.
[Has 97] W.C. Hasz, C.A. Johnson and M.P. Borom, U.S. Patent No. 5660885 (1997).
[Has 99] W.C. Hasz, M.P. Borom and C.A. Johnson, U.S. Patent No. 5871820 (1999).
[Hea 94] Peter J. Heaney, Structure and chemistry of the low-pressure silica polymorphs. Reviews in Mineralogy and Geochemistry 29 (1994) 1–40.
[Hel 05] D.A. Helmick, G.H. Meier, F.S. Petit, Met. Mat. Trans. A, 36 (2005), 3371.
[Hen 93] Henager, Jr.,C.H., Brimhall, J. L., et al. (1993). Structural Intermetallics. TMS, Warrendale, PA.
[Her 88] W. Hertl, J. Appl. Phys., 63, 5514-5520 (1988).
[Hes 95] P.C. Hess Thermodynamic Mixing Properties and the Structure of Silicate Melts. In: Structure, Dynamics & Properties of Silicate Melts. Edited by Stebbins JF, McMillan PF, Dingwell DB, vol. 32. Chelsea, MI: Mineralogical Society of America; 1995: 145-189.
[Heu 90] A.H. Heuer, V.L.K. Lou, J. Am. Ceram. Soc. 73, 2789-2803 (1990)
[Hig 94] John B. Higgins, Silica zeolites and clathrasils, Reviews in Mineralogy and Geochemistry 29 (1994) 507–543.
[Hin 76] J.W. Hinze, H.C. Graham, J. Electrochem. Soc. 123, 1066-73 (1976)
[Ina 96] Inaba, H. and H. Yokokawa (1996). J. Phase Equilibria 17: 278.
[Jac 93] N.S. Jacobson, J. Am. Ceram. Soc. 76, 3-28 (1993)
[Jac 05] Jacobson, N, et.al., J. Chem. Thermodynamics 37 1130–7 (2005).

[Jac 08] N.S. Jacobson, D.J. Roth, R.W. Rauser, J.D. Cawley, D.M. Curry, Surf. Coat. Tech. 203, 372-83 (2008)
[Jac 11] N.S. Jacobson, D.L. Myers, Oxid. Met. 75, 1-25 (2011)
[Jac 13] N Jacobson, B Harder, D Myers. Oxidation Transitions for SiC Part I. Active-to-Passive Transitions. J Am Ceram Soc 2013, 96(3):838-844.
[Jeh 05] Jehanno P, Heilmaier M, Kestler H, Bo¨ning M, Venskutonis A, Bewlay B, et al. Metall Mater Trans A 2005;36:515.
[Jia 07] Z.Q. Jiang, W.X. Huang, Z. Zhang, H. Zhao, D.L. Tan, X.H. Bao, Surf Sci, 601 (2007) 844-851.
[Kae 11] J. Kaewkhao, W. Siriprom, S. Insiripong, T. Ratana, C. Kedkaew, P. Limsuwan, J. of Phys.: Conf. Ser., 266 (2011) 012012.
[Kaw 64] Kawasaki, K., Senzaki, K., Tsuchiya, I., J. Coll. Sci., 19, p.144-51 (1964).
[Kie 91] Kieschke, R. R., R. E. Somekh, et al. (1991). "Acta Metall." 39: 427.
[Kim 06] Kim, S. and J. H. Perepezko (2006). J. Phase Equilibria 6(27): 605-613.
[Kim 91] Kim, Y. W. and D. M. Dimiduk (1991). JOM 43: 40.
[Kin 94] Kathleen J. Kingma, Russell J. Hemley, Raman spectroscopic study of micro crystalline silica American Mineralogist, 79, (1994) 269-273.
[Kir 92] Kir, T. A. and E. L. Courtright (1992). Mat. Sci. & Eng. A A155: 67 - 74.
[Kir 87] Kirkaldy, J. S. and D. J. Young (1987). Diffusion in the Condensed State. London, UK, Institute of Metals.
[Kof 88] Kofstad, P. (1988). High Temperature Corrosion,. London, Elselvier Applied Science Publishers LTD.
[Kon 76] W.L. Konijnendijk, J.M. Stevels, the structure of borosilicate glasses studied by Raman scattering, J. non-crystalline solids. 20, (1976) 193-224.
[Kra 06] S. Kramer, J. Yang, and C.G. Levi, J. Am. Ceram. Soc. 89, 3167 (2006).
[Kra 08] Kramer, S., et al., Mat. Sci. Eng. A, 2008. **490**(1-2): p. 26-35.
[Kur 07] K. Kurokawa, A. Yamauchi, Solid State Phenomena, 127 (2007) 227-232.
[Lam 92] Lamkin, M. A., F. L. Riley, et al. (1992). Journal of European Ceramic Society 10: 348.
[Law 90] Lawson, M. G., Kim, H. R., Pettit, F. S. & Blachere, J. R. Hot Corrosion of Silica. *J. Am. Ceram. Soc.* **73,** 989–995 (1990).
[Leb 93] P.P. Leblanc and R.A. Rapp, J. Electrochem. Soc., 140, L41-L43 (1993).
[Lev 74] Levine, S. R., Caves, R.M., J. Electrochem. Soc. 1974, 121, 1051.
[Lev 11] I. A. Levitskii and L. F. Papko, "Effect of composition and structural factors on the viscosity of borosilicate glasses and melts," *Glass Ceram.*, vol. 67, no. 11, p. 336, Apr. 2011.
[Lid 03] David R. Lide, "Standard Thermodynamic Values," in *CRC Handbook*, 84th ed., Boca Raton, Flordia: CRC Press, 2003, pp. 5:5-5:60,5:85-5:86.
[Loo 90] Loo, F. J. J. v. (1990). Prog. Solid St. Chem. 20: 47.
[Loo 83] Loo, F. J. J. v. and G. F. Bastin (1983). DIMET4 - 82: Diffusion in Metal and Alloys. Trans. Tech. Pub., MA.
[Loo 85] Loo, F. J. J. v., J. A. v. Beek, et al. (1985). Solid St. Ionics 16: 131.
[Lup 83] Lupis, C. H. P. (1983). Chemical Thermodynamics of Materials,, Elsevier Science Pub., New York, NY,: 53.
[Mai 79] Maier, K., H. Mehrer, et al. (1979). Z. Metallkde. 90: 271.

[Man 04] Mandal, P., Kramer M, et. al., Materials Science and Engineering A 371 pp.335–42 (2004)
[Mar 71] Marakushev AA, Bezmen NI, International Geological Review, **13**(12):1781-1794(1971).
[McH 96] McHale, A. E. and R. S. Roth (1996). Phase Equilibria Diagrams 12: 11.
[McM 82] P. McMillan, B. Piriou, J. Non-Cryst. Solids 53, 279-98 (1982)
[Mek 96] A. Mekki, D. Holland, C. F. McConville, M. Salilm, J. Non-Cryst. Solids. 208 (1996) 267-76.
[Men 93] Mendiratta, M. G. and D. M. Diminuk (1993). Metall. Trans. 24A: 501.
[Men 02]Mendiratta, M. G., T. A. Parthasarathy, et al. (2002). "Oxidation behavior of aMo-Mo3Si-Mo5SiB2 (T2) three phase system." Intermetallics 10: 225-232.
[Mer 05] C. Mercer, S. Faulhaber, A.G. Evans and R. Darolia, Acta Mater. 53, 1029 (2005).
[Mes 60] DJ. Meschi, W.A. Chupka, and J. Berkowitz, J. Chem. Phys., 33 (2), pp. 530-3 (1960)
[Mey 96] Meyer, M. K. and M. Akinc (1996). "Oxidation Behavior of Boron-Modified Mo5Si3 at 800-1300C." Journal of the American Ceramic Society 79(4): 938-944.
[Mey 99] Meyer, M. K., A. J. Thom, et al. (1999). "Oxide scale formation and isothermal oxidation behavior of Mo-Si-B intermetallics at 600-1000°C." Intermetallics 7: 153-162.
[Mit 07] R. Mitra, S. Paswan, S.K. Roy, Intermetallics 15, 1217-27 (2007)
[Mue 92] Mueller, A., G. Wang, et al. (1992). "Oxidation behavior of tungsten and germanium-alloyed molybdenum disilicide coatings." Materials Science & Engineering A155: 199-207.
[Muk 02] Mukundhan, P., Du, H. H. & Withrow, S. P. Sodium-Accelerated Diffusion of Magnesium in Silica and Its Retardation by Aluminum. *J. Am. Ceram. Soc.* **85,** 1613–1615 (2002).
[Mys 83] B. O. Mysen, "The Structure of Silicate Melts", Ann. Rev. Earth Planet. Sci. 1983 [11] 75-97
[Mys 85] B. O. Mysen, D. Virgo and F. A. Seifert," Relationship between properties and structure of aluminosilicate melts", American Mineleralogist, 1985 [70] 88-105.
[Nat 00] Natesan, K. and S. C. Deevi (2000). "Oxidation behavior of molybdenum silicides and their composites." Intermetallics 8: 1147-1158.
[Nes 11] H. W. Nesbitt, et al., J. Non-Cryst. Solids, 357 (2011) 170-80.
[Nic 92] K.G. Nickel, J. Eur. Ceram. Soc. 9, 3-8 (1992)
[Nis 10] http://www.ctcms.nist.gov/oof/oof2/ (2010).
[Now 57] Nowotny, H., E. Dimakopoulou, et al. (1957). Monatshefte Fuer Chemie 88: 180.
[Nun 00] Nunes, C. A., R. Sakidja, et al. (2000). Intermetallics 8: 327.
[Nun 97] Nunes, C. A., R. Sakidja, et al. (1997). Phase stability in high temperature Mo-rich Mo-Si-B alloys. Structural Intermetallics 1997. M. V. Nathal, R. Darolia, C. T. Liuet al. Warrendale, PA, TMS: 831-839.
[Opi 95] E.J. Opila, N.S. Jacobson, Oxid. Met. 44, 527-44 (1995)
[Opi 97] Opila, E, et. al., J. Am. Ceram. Soc., 80 [1] 197-205 (1997)
[Opi 03a] Opila, E., et. al. , J. Am. Ceram. Soc., 86[8] 1238-48 (2003)
[Opi 03b] Oplia, E, et. al., J. Am. Ceram. Soc., **86** [8] 1256–61 (2003)
[Opi 06] E. J. Opila, N. S. Jacobson, D. L. Myers, E. H. Copland, JOM, Jan. 2006, p.22 (2006)
[Opi 11] E.J. Opila, M.K. Boyd, Mat. Sci. Forum 696, 342-7 (2011)
[Ots 90] N. Otsuka and R.A. Rapp, J. Electrochem. Soc., 137, 53-60 (1990).
[Pad 02} N.P. Padture, M. Gell, and E.H. Jordan, Science, 296, 280-4 (2002).

[Par 02a] Parthasarathy, T. A., M. G. Mendiratta, et al. (2002). "Oxidation mechanisms in Mo-reinforced Mo5SiB2(T2)-Mo3Si alloys." Acta Materialia 50: 1857-1868.
[Par 02b] J. S. Park, R. Sakidja, J. H. Perepezko, Scripta Mater. 2002, 46, 765.
[Per 93] Perepezko, J. H. (1993). Composite Interfaces 1: 463.
[Per 95] Perepezko, J. H., M. H. d. S. Bassani, et al. (1995). Mat. Sci. & Eng. A 195: 1.
[Per 97] Perepezko, J. H., C. A. Nunes, et al. (1997). High Temperature Ordered Intermetallic Alloys VII. A. Wanner. Pittsburgh, PA, MRS: 1.
[Per 98] Perepezko, J. H., J. S. Park, et al. (1998). Mat. Res. Soc. Symp. Proc. 48: 509.
[Per 05] J.H. Perepezko, R. Sakidja, J.S. Park, J. Hamann, Scripta Mater. 53, 723-8 (2005)
[Per 06] J. H. Perepezko, J. S. Park, R. Sakidja, US Patent 7,005,191 (2006).
[Per 08] J. H. Perepezko, F. Rioult, R. Sakidja, Mat. Sci. Forum 2008, 595, 1065.
[Per 10] J.H. Perepezko, R. Sakidja, JOM 62, 13-19 (2010).
[Per 12] J.H. Perepezko, J.M. Bero, R. Sakidja, I.G. Talmy, J. Zaykoski, Surf Coat Tech, 206 (2012) 3816-3822.
[Pet 11] F. Petit, Oxid Met., 76, 1-21 (2011).
[Py 77] M.A. Py, P_H. E. Schmid, J.T. Vallin, Raman scattering and structural properties of MoO_3 Nuovo Cimento, 38B (1977) 271-279.
[Ram 03] C. Ramachandra, K. N. Lee and S.N. Tewari, Sur. Coat Tech, 172, 150-157 (2003).
[Ram 85] Ramkers, P. P. J., F. J. J. v. Loo, et al. (1985). Solid State Ionic 16: 179.
[Rap 73] Rapp, R. A., A. Ezis, et al. (1973). Metall. Trans. A4: 1283.
[Rap 86] R.A. Rapp, Corrosion, 42, 568-577 (1986).
[Ree 06] Reed, R.C., JOM, 2006. **58**(1): p. 36-36.
[Ric 12] S. Richter and J. Mayer, "Sample Preparation for EPMA - EMAS 2012 - 10th Regional Workshop on Electron Probe Microanalysis Today - Practical Aspects," Padua, Italy, (2012).
[Rio 05] Rioult F, Sekido N, Sakidja R, Perepezko JH. J Electrochem Soc 2007;154:C692.
[Rio 09] F.A. Rioult, S.D. Imhoff, R. Sakidja, J.H. Perepezko, Acta Mater. 57 (2009) 4600-13.
[Rit 12] P. Ritt, R. Sakidja, J.H. Perepezko, Surf. Coat. Tech. 206, 4166-72 (2012)
[Ros 87] Ross, E. R. and C. T. Sims (1987). Superalloys II. C. T. Sims. New York, NY, John Wiley & Sons, Inc.: 97.
[Rye 85] Ryerson FJ, Geochim Cosmochim Ac, **49**(3):637-649 (1985).
[Sak 98] Sakidja, R., H. Sieber, et al. (1998). Molybdenum and Molybdenum Alloys. A. Crowson, E. S. Chen, J. A. Shield and P. R. Subramanian. Warrendale, PA, TMS: 99.
[Sai 07] E. Saiz *et al.*, "Nonreactive spreading at high temperature: Molten metals and oxides on molybdenum," *Phys. Rev. E*, vol. 76, no. 4, p. 041602, Oct. 2007.
[Sak 99] Sakidja, R., H. Sieber, et al. (1999). Phil. Mag. Lett. 79: 351.
[Sak 05] R. Sakidja, J. S. Park, J. Hamann, J. H. Perepezko, Scr. Mater. 2005, 53, 723.
[Sak 08] R. Sakidja, J.H. Perepezko, S. Kim, N. Sekido, Acta Mater. 56, 5223-44 (2008).
[Sat 04] Sato, R., Tomozawa, M., J. Non-Cryst. Sol., 343, p.26-32 (2004).
[Sch 11] Scheidema, M. N. & Taskinen, P. Decomposition Thermodynamics of Magnesium Sulfate. *Ind. Eng. Chem. Res.* **50,** 9550–9556 (2011).
[Sch 99] Schneibel, J. H., C. T. Liu, et al. (1999). "Microstructure and mechanical properties of Mo-Mo3Si-Mo5SiB2 silicides." Materials Science & Engineering A261: 78-83.
[Sch 91] H. Scholze, Glass: Nature, Structure and Properties, Springer-Verlag, New York, 1991.

[Sch 98] Schneibel, J. H., C. T. Liu, et al. (1998). Scripta Mater. 38: 1169.
[Sch 05] Schneibel JH, Ritchie RO, Kruzic JJ, Tortorelli PF. Metall Mater Trans A 2005;36:525.
[Sha 95] Shah, D. M., D. L. Anton, et al. (1995). Mater. Sci. Eng. A A192/193: 658.
[Sha 92] Shah, D. M., D. Berczik, et al. (1992). Mater. Sci. and Eng. A155: 45.
[Shi 86] D-Z. Shi and R.A. Rapp, J. Electrochem. Soc., 133, 849-850 (1986).
[Shi 93] Shiota, I. (1993). Critical Issues in the Development of High Temperature Structural Materials. N. S.
Stoloff, D. J. Duquette and A. F. Giamei. Warrendale, PA, TMS: 303.
[Sik 80] V.K. Sikka, C.J. Rosa, Corros Sci, 20 (1980) 1201-&.
[Sim 55] M. Simnad, A. Spilners, J. of Metals, 7 (1955) 1011 - 1016.
[Sin 91] Singh, M. and H. Wiedemeier (1991). J. Am. Ceram. Soc. 74: 724.
[Smi 84] Smith, P. R. and F. H. Froes (1984). "J. Metals." 36(Mar): 19.
[Spi 04] I. Spitsberg, J. Steibel, Int. J. Appl. Ceram. Tech. 1, 291-301 (2004)
[Sto 87] Stoloff, N. A. (1987). Superalloys II. C. T. Sims. New York, NY, John Wiley & Sons, Inc.: 61.
[Str 98] J. Stringer, "Coatings in the electricity supply industry: past, present, and opportunities for the future," *Surf. Coat. Technol.*, vol. 108–109, pp. 1–9, Oct. 1998.
[Str 93] Strum, M. J. and G. A. Henshall (1993). in High Temperature Ordered Intermetallic Alloys V. Mater. Res. Soc. Proc., Pittsburgh, PA.
[Sum 17] J. Sumner, Q. Aksoul, J. Delgado, A. Potter, and S. Gray, "Impact of Deposit Recoat Cycle Length on Hot Corrosion of CMSX-4," *Oxid. Met.*, vol. 87, no. 5–6, pp. 767–778, Jun. 2017.
[Tay 17] Taylor, M. & Perepezko, J. H. Hot Corrosion of Mo–Si–B Coatings. *Oxid. Met.* **87,** 705–715 (2017).
[Ted 66] Tedmon Jr., C. S. ,J. Electrochem. Soc. p.766-8 (1966).
[Tho 93] Thom, A. J., M. K. Meyer, et al. (1993). Processing and Fabrication of Advanced Material for High Temperature Applications III. T. S. Srivitsan and V. A. Ravi. Warrendale, PA, TMS: 413.
[Tho 02] Thom, A. J., E. Summers, et al. (2002). "Oxidation behavior of extruded Mo5Si3Bx-MoSi2-MoB intermetallics from 600°C-1600°C." Intermetallics 10: 555-570.
[Vas 92] Vasudevan, A. K. and J. J. Petrovic (1992). Mater. Sci. and Eng. A155: 1.
[Vas 00] R. Vassen, X. Cao, F. Tietz, D. Basu and D. Stover, J. Am. Ceram. Soc., 83, 2023 (2000).
[Vau 90] W.L. Vaughn, H.G. Maahs, J. Am. Ceram. Soc. 73, 1540-3 (1990)
[Wag 38] Wagner, C. (1938). Z. Anorg. Allgem. Chem 236: 320.
[Wag 58] C. Wagner, J. Appl. Phys. 29, 1295-7 (1958)
[Wan 06] Wang, Y., Y. Sohn., et al. (2006). J. of Phase Equilibria and Diffusion 27(6): 671.
[Whi 83] Whittle, D. P. (1983). High Temperature Corrosion. NACE-3. R. A. Rapp. CA, National Association of Corrosion Engineers: 171.
[Woo 03] Woodard, S. R., R. Raban, et al. (2003). Oxidation resistant molybdenum. United States Patent. United States of America, United Technologies Corporation.
[Yan 96] Yanagihara K, Maruyama T, Nagata K. Intermetallics, **4**:S133-S139 (1996).
[Yaz 06] Yazhenskikh E, Hack K, Muller M, Calphad, **30**(3):270-276 (2006).
[Yaz 08} Yazhenskikh E, Hack K, Muller M: Calphad, **32**(1):195-205.(2008)
[Yoo 06] J.K. Yoon, K.W. Lee, S.J. Chung, I.J. Shon, J.M. Doh, G.H. Kim, J Alloy Compd, 420 (2006) 199-206.
[Yos 02] Yoshimi, K., S. Nakatani, et al. (2002). "Oxidation behavior of Mo5SiB2-based alloy at elevated temperatures." Intermetallics 10: 407-414.

[You 58] Young, G.J., J. Coll. Sci., 13, p.67-85 (1958).
[Yug 12] S. Yugeswaran, A. Kobayashi and P.V. Ananthapadmanabhan, Mater. Sci. Eng. 177B,536-542 (2012).
[Zel 95] Zeller, R. et.al. Phys. Rev. B 52, 8807–8812 (1995).
[Zhe 12] Zheng QJ, Smedskjaer MM, Youngman RE, Potuzak M, Mauro JC, Yue YZ, Appl Phys Lett, **101**(4) (2012).